Nature Communications

https://doi.org/10.1038/s41467-026-73434-0

Article in Press

Host mature tRNAome as a decoding switch regulates antiviral and proviral responses

Received: 4 August 2025

Accepted: 8 May 2026

Cite this article as: Ou, X., Lin, X., Chen, J. *et al.* Host mature tRNAome as a decoding switch regulates antiviral and proviral responses. *Nat Commun* (2026). https://doi.org/10.1038/s41467-026-73434-0

Xumin Ou, Xiaoming Lin, Jiayi Chen, Wenwen Yang, Di Sun, Shun Chen, Mafeng Liu, Dekang Zhu, Mingshu Wang, Renyong Jia, Sai Mao, Ying Wu, Qiao Yang, Shaqiu Zhang, Xinxin Zhao, Juan Huang, Bing Tian, Zhen Wu, Yu He, Qiuwei Pan & Anchun Cheng

Host Mature tRNAome as a Decoding Switch Regulates Antiviral and Proviral Responses

Xumin Ou [1,2,3,4,5#], Xiaomin Lin [1,2,5#], Jiayi Chen [1,2,5#], Wenwen Yang[1,2,5#], Di Sun[1,2,5], Shun Chen [1,2,4,5], Mafeng Liu [1,2,5], Dekang Zhu [1,2,5], Mingshu Wang [1,2,5], Renyong Jia [1,2,5], Sai Mao [1,2,5], Ying Wu [1,2,5], Qiao Yang [1,2,5], Shaqiu Zhang[1,2,5], Xinxin Zhao[1,2,5], Juan Huang [1,2,5], Bing Tian [1,2,5], Zhen Wu [1,2,5], Yu He [1,2,5], Qiuwei Pan [3], Anchun Cheng [2,5,6*].

[1]Agricultural Animal Diseases and Veterinary Public Health Key Laboratory of Sichuan Province, Sichuan Agricultural University, Chengdu, Sichuan, China

[2]Engineering Research Center of Southwest Animal Disease Prevention and Control Technology, Ministry of Education of the People's Republic of China, Sichuan Agricultural University, Chengdu, Sichuan, China

[3]Department of Gastroenterology and Hepatology, Erasmus MC – University Medical Center Rotterdam, PO Box 2040, NL-3000 CA Rotterdam, The Netherlands

[4]Key Laboratory of Agricultural Bioinformatics, Ministry of Education, China

[5]Institute of Veterinary Medicine and Immunology, College of Veterinary Medicine, Sichuan Agricultural University, China

[6]State Key Laboratory of Green Pesticide, GuiZhou University, GuiYang, China

[#]These authors contributed equally.

*Corresponding author: Anchun Cheng, chenganchun@vip.163.com

Abstract

Current virus-host studies primarily concentrate on the battle race at the levels of mRNA transcription and protein translation. These processes, on both the host and virus sides, rely on the mature tRNAome to decode, yet they remain largely unexplored. In this study, we report a previously unrecognized dichotomy in the host tRNAome concerning antiviral and proviral responses. We demonstrate that the host's mature tRNAome, which is coupled with amino acid metabolism, is dynamically remodeled by interferon-alpha (IFN-α) and regulates the translation efficiencies of downstream interferon-stimulated genes (ISGs). Interference with tRNAome maturation or charging dampens the antiviral efficacy of IFN-α in hepatitis E virus (HEV)-infected cells. In contrast, hepatitis B virus (HBV) infection, which does not induce the ISG response, still remodels the host tRNAome to promote its own infection, particularly through tRNA-Arg-UCU. Both charging and genetic interference with tRNA-Arg-UCU inhibit HBV DNA replication, while its overexpression *in vitro* and in a male mouse model enhances HBV DNA replication and translation. Importantly, this tRNA not only facilitates the decoding of the nucleocapsid, where HBV replication initiates, but also indirectly affects pregenomic RNA (pgRNA) transcription, which encodes the nucleocapsid subunit, core protein. These findings suggest the potential for tRNA-based strategies to amplify the interferon response and develop antivirals targeting HBV.

Introduction

During the ongoing evolutionary arms race between viruses and their hosts, multiple layers of competition regulate the outcome. Current research primarily focuses on the layers of transcription and translation, which constitute a conventional gene–protein production line[1, 2, 3, 4, 5, 6]. Viruses within infected cells can often inhibit host gene transcription[2] and shut off host translation[7], manipulating host machinery for their own benefit[1, 8]. Simultaneously, the infected host cells can initiate an innate immune response to fight back, primarily through the production of interferons[9]. Once secreted, interferons create a defense state by activating hundreds of interferon-stimulated genes (ISGs). These ISGs, with specific or broad antiviral activities, can target multiple steps during the viral life cycle[9, 10, 11], thereby efficiently inhibiting viral infection[9, 12]. However, the conventional gene-protein production line on both the virus and host sides relies on the host tRNAome[13, 14], which serves as a crucial regulator between the cellular or viral transcriptome and proteome. Consequently, the host tRNAome may be exploited to coordinate host antiviral response or, conversely, to enhance viral infection. Nevertheless, how the host tRNAome acts as a potentially decoding “switch” in the two competitive processes remains largely unexplored.

Within the ribosome, the mature tRNAome facilitates the translational decoding of virtually all mRNAs, regardless of whether they are derived from the host or from viruses. Theoretically, 61 types of aminoacyl-tRNAs are required to decode all genetic codes that specify 20 amino acids (AAs)[15, 16]. However, the minimal tRNA species required for life are usually fewer than the theoretically calculated number due to the wobble decoding rule[14, 17]. In the human genome, there are roughly 600 tRNA gene loci consisting of 57 tRNA isodecoders[18]. The transcription of tRNA genes is initiated by the binding of the transcription factors TFIIIC and TFIIIB to the A and B boxes, which serve as unique internal promoters for tRNA, while correspond to the tRNA D-loop and TΨC loop[19]. RNA polymerase III (Pol III) is then recruited to the TFIIIB-DNA complex, initiating the

transcription of pre-tRNAs[20]. The pre-tRNAs undergo post-transcriptional processing to remove additional leader sequences and to add a common 3'-CCA ribonucleotide, ultimately becoming mature tRNAs[17]. The CCA tail serves as a universal site for the charging of each amino acid, with the charging process catalyzed by aminoacyl-tRNA synthetases (aaRSs)[15].

Interferon-alpha (IFN-α) is a clinically used antiviral drug for treating viral hepatitis, including infections caused by the hepatitis B virus (HBV)[21] and the hepatitis E virus (HEV)[22]. After binding to its receptor, interferon initiates a signal transduction cascade and triggers the transcription of numerous ISGs[3, 4, 21]. The transcription of these ISGs is mediated by the conserved Janus kinase/signal transducer and activator of transcription (JAK-STAT) signaling pathway, alongside other noncanonical pathways[3, 4, 23]. With a continuous supply of the mature tRNAome to the host ribosome, these ISG transcripts will be translated into proteins, which then exert antiviral effects through various mechanisms[11], although many of these ISGs remain not fully understood.

HBV is a DNA virus belonging to the *Hepadnaviridae* family; annually, hepatitis B results in nearly 900,000 deaths, causing a significant disease burden[24, 25]. Unlike many other viruses, HBV infection does not trigger an ISG response due to its stealth properties[26], rendering it largely invisible to the host immune system. Despite this, all viruses, including HBV, depend completely on the host's mature tRNAome to produce viral proteins. Consequently, HBV may preferably exploit the host's tRNAome for its own advantage, rather than to promote host antiviral responses, particularly when ISG responses are defective or nonresponsive[26]. In this regard, tRNA molecules may represent an inventive target for the development of anti-HBV drugs, although the draggability of tRNAs has primarily been scrutinized in certain cancers[16, 27] and genetic diseases[28].

Emerging evidence indicates that the mature tRNAome is not as static as previously expected; rather, it can be modulated in various pathophysiological scenarios[29], including

cancer development[27], inflammatory responses[30, 31] and viral infection[17, 32, 33]. Based on these observations and the reliance on the mature tRNAome in the virus-host interaction, we hypothesize that the tRNAome's landscape maybe conditionally modulated to orchestrate either host antiviral responses or viral infection.

Here, we show that the mature tRNAome is dynamically remodeled by IFN-α, which in turn regulates the translation efficiency (TE) of numerous ISGs and influences the resulting antiviral effect. Conversely, HBV infection, which does not induce an ISG response, also remodels the host mature tRNAome, particularly the conserved tRNA-Arg-UCU, to facilitate multiple stages of infection, ranging from viral protein synthesis to DNA replication and pgRNA transcription. This study reveals an unrecognized dichotomy of the host tRNAome, serving as a decoding switch that bilaterally orchestrates anti-viral and proviral responses.

Results

Interferon-α dynamically orchestrates the antiviral gene-protein production line.

The antiviral gene-protein production line that follows the interferon response consists of two sequential biological processes: the transcription of ISGs and their protein synthesis (Fig. 1a). Upon treatment with IFN-α 2b (hereafter, referred to as IFN-α), robust transcriptional upregulation of many ISGs was observed (Supplementary Fig. 1a), which is consistent with previous observations[22, 34]. After 24 h of treatment, the abundance of total cellular protein did not show a visible change (Supplementary Fig. 1b), and it even showed a reduction of 5.82% after 48 h (Supplementary Fig. 1c-d). Overall, ISG transcription appears to be globally strong, while cellular protein synthesis seems to be rewired as well.

To study the dynamic coordination between the ISG transcriptome and proteome from 4 to 24 h, high-throughput mRNA sequencing (RNA-seq) was combined with the quantitative proteomic mass spectrometry (MS) analysis using TMTpro 16-plex

technology (Supplementary Fig. 2a). In total, approximately 14,000 mRNAs and 5,000 proteins were identified (Supplementary Table 1, Fig. 1b-e). For the transcriptome, a large number of ISGs were robustly upregulated and dynamically changed over time (Fig. 1b-c). At 4, 8, and 24 h, 313, 468, and 360 ISGs were respectively identified at the mRNA level [fold change (FC) > 2.0] (Supplementary Fig. 2b). Furthermore, we observed dynamic changes in the proteome (Fig. 1d); however, only 36 out of these proteins were consistently identified and ultimately upregulated at 24 h (Fig. 1e). In total, 29, 214 and 434 upregulated ISG candidates were identified by proteomic MS after 4, 8 and 24 h of treatment (FC > 1.2) (Supplementary Fig. 2c).

Using the ISG candidates identified by RNA-seq and proteomic MS, Pearson correlation analyses were performed to study their cross-omic coordination (Fig. 1f-h, Supplementary Fig. 2d). From 4 to 24 h, the Pearson correlation coefficients (Rs) between the ISG transcriptome and proteome gradually increased to 0.72 (p value = 1.94e-90), while the R values at 8 and 4 h were relatively low (Fig. 1f, g). Since transcription may precede protein translation, we specifically investigated whether a lagging effect exists between the early mRNA response (input) and subsequent protein synthesis (output). For instance, we analyzed the coordination strength between the ISG transcriptomic data at 4 h and the protein data at 8 h, and so forth (Fig. 1i-k). As expected, a lagging effect was observed between the ISG transcriptomic data at 8h and the ISG proteomic data at 24 h (R = 0.73, p = 4.96e-92) (Fig. 1j), as well as between the ISG transcriptomic FCs at 4h and the ISG proteomic fold changes at 24 h (R = 0.70, p = 2.41e-82) (Fig. 1k). However, the effect was relatively small between the ISG mRNA FCs at 4h and the protein FCs at 8 h (R = 0.45, p = 2.41e-28) (Fig. 1i). Although a lagging effect was observed, the ISG proteomic response was relatively weaker than the ISG transcriptome during the treatment (Fig. 1l, Supplementary Fig. 2d).

Next, we measured the TEs (defined as the ratios of protein/mRNA FCs) of all genes[35], and found that the genome-wide TEs at 8 and 24 h were significantly different

compared to those at 4 h (n = 4191) (Fig. 2a). Among these, 572 genes (mostly ISGs) exhibited lower TEs, below 1.0 (Fig. 2a). With quantitative mRNA and protein data for the 36 ISGs (defined as “core ISGs”), we further depicted their TE dynamics (Fig. 2b). As observed, their TEs dynamically changed over time. From 4 to 8 h, their TEs either substantially decreased or did not change, while they dramatically increased from 8 to 24 h (Fig. 2b). Notably, the TEs of these core ISGs were generally low, with most not exceeding 50%; in fact, many of the ISGs could only be detected by RNA-seq (Fig. 1l). Collectively, the ISG transcriptomes and proteomes are dynamically rewired upon IFN treatment.

Remodeling of the mature tRNAome modulates translational decoding of ISGs.

We hypothesized that the mature tRNAome, if remodeled, could regulate overall ISGs’ TEs, and affect their antiviral efficacy[36, 37]. Previously, we developed a tailored approach to quantify the entire mature tRNAome[17, 30]. Through a deacylation reaction, the AAs charged on tRNAs are removed, thus allowing for the quantification of entire mature tRNAome. Using this method, we profiled the landscape of the host tRNAome from 4 to 48 h of IFN-α (1000 IU/mL) treatment, and found that the mature tRNAome was robustly and dynamically remodeled (Fig. 2c). From 4 to 8 h, the mature tRNAome was significantly downregulated compared to control groups; later, the mature tRNAome gradually recovered to normal levels from 8 to 24 h (Fig. 2d). At a physiologically relevant concentration of 10 IU/mL, we still observed a downregulation of many tRNAs during treatment (Fig. 2e), though not to the same extent as at 1000 IU/mL.

Combining the ISG TEs and the mature tRNAome data, a clear interplay between tRNAome availability and ISG translation was found (Fig. 2b, d). When the mature tRNAome decreased (Fig. 2d), the TEs of many ISGs extensively decreased (Fig. 2b). When the mature tRNAome recovered (Fig. 2d); their TEs dramatically increased (Fig. 2b), showing that the availability of the mature tRNAome regulates the translation of ISGs (Fig. 2f). Furthermore, we investigated the underlying mechanisms supporting tRNAome

functionality. This was performed through the analysis of the mRNA and protein FC data related to: (a) tRNA processing, (b) translation initiation/elongation factors and (c) ribosomal components (Fig. 2g). Except for EIF2AK2 which was also identified as a core ISG candidate (Fig. 2g), these protein-coding genes did not respond to IFN-α at the mRNA and protein levels (Fig. 2g).

When the mature tRNAome is remodeled, cellular AA metabolism should be modulated, as tRNAs, which serve as adaptors for AAs, are altered[38]. The metabolic changes in hepatocytes following 8 h of IFN-α treatment were analyzed. We found that hundreds of metabolites were altered upon treatment (Supplementary Fig. 3a). Among them, many AA-related metabolites were changed (Supplementary Fig. 3b). KEGG analysis coherently indicated that 14 out of the 20 AA metabolism-related pathways were significantly suppressed, including glycine, serine and threonine metabolism (Supplementary Fig. 3c-d). These data demonstrate that the intracellular AA metabolism is also rewired when the mature tRNAome is remodeled.

Using ribosome profiling, which captures a real-time translational decoding of genomic ISGs (Fig. 3h), we observed a similar translation dynamic for many ISGs, characterized by ribosome translating mRNA abundance (Fig. 2i). Importantly, all 36 core ISGs were recaptured, and a similar TE dynamic was observed (Fig. 2j). Through a cumulative input-and-output analysis (Fig. 2b) and real-time capture of ISG translational decoding (Fig. 2h), our data show that the remodeling of the mature tRNAome orchestrates the translational decoding of ISGs.

tRNA transcription participates in interferon-mediated tRNAome remodeling.

Next, we investigated whether tRNA gene transcription is involved in the remodeling of the mature tRNAome. We utilized a reporter plasmid by sequentially inserting elements that mediate the transcription of tRNA genes (Fig. 2k, Supplementary Fig. 4). Similar to the trend observed in IFN-α-mediated tRNAome remodeling, tRNA transcription activity also exhibited a sequential pattern of suppression and relief (Fig. 2l). This phenomenon

is closely correlated with the transcriptional competition between RNA polymerase II (Pol II) and RNA polymerase III (Pol III), which respectively transcribe protein-encoding genes (ISGs) and tRNA genes[39]. Consistent with this, when ISG transcription is highly active at 8 h (Fig. 1c), a downregulation of the mature tRNAome is observed (Fig. 2c-e), and vice versa at 24 h. Similarly, a downregulation of the mature tRNAome was also observed when high transcription of proinflammatory genes was observed in our previous investigations[30 31].

SLFN11 is an interferon-stimulated tRNA endonuclease that primarily cleaves type 2 tRNAs, as reported[40]. We tested whether SLFN11 knockdown alleviates the downregulation of the mature tRNAome (Fig. 2m), focusing on the type 2 tRNA-Ser and tRNA-Ile families, along with four type 1 tRNAs. However, no mitigation of tRNA downregulation was observed (Fig. 2n). Notably, in liver tissues, hepatocytes have relatively low SLFN11 protein levels, according to the Human Protein Atlas archives. Additionally, an upregulation of SLFN11 at the mRNA or protein levels was not observed in the present datasets, suggesting alternative pathways for tRNAome downregulation. Nevertheless, tRNA transcription suppression and its transcriptional competition with ISGs likely play a role (Fig 2k-l).

The highly biased codons of ISGs dampen the complementarity between the tRNAome supply and the decoding needs of ISGs.

The decoding efficiency of the tRNAome, besides its abundance, is intimately linked to mRNA codon usage. A gene with rare codons and a low number of paired tRNAs often results in translation slowdown or termination[13, 41]. This motivated us to investigate the complementarity between the tRNAome and ISG codons. Unexpectedly, we found that IFN-α mediated tRNAome remodeling is less compatible with the codons of ISGs (Supplementary Fig. 5a), and does not fit the supply-need rule based on the translation hypothesis[1, 42]. All correlation coefficients (Rs) are less than 0.40, implying that a maximum of 40% of the variations in codon usage can be explained by the known

tRNAome abundances. Not only do these core ISGs (Supplementary Fig. 5b), but also the consensus annotated ISGs triggered by IFN-α, β and γ (Supplementary Fig. 5c-e) exhibit a highly biased codon usage pattern. Theoretically, the biased codons of ISGs require a biased remodeling of the mature tRNAome to amplify decoding efficiencies[43]. However, all tRNA species were globally remodeled, making it challenging to achieve this match.

Additionally, there are 85 unusual ISGs that do not exhibit changes at the mRNA level (Supplementary Fig. 6a), yet their protein levels were ultimately elevated after 24h (Supplementary Fig. 6b). Their TEs should be more directly influenced by the mature tRNAome (Supplementary Fig. 6c). Similar to the codon-tRNA correlations of the core ISGs (Supplementary Fig. 5a), we again found low codon-tRNA correlations for these unusual ISGs (Supplementary Fig. 6d), coupled with a highly biased codon pattern (Supplementary Fig. 6e). Thus, in addition to tRNAome availability, the codon bias of ISGs in genetics may contribute to their translational control. Nevertheless, their codon usage is highly biased, dampening their complementarity with tRNA abundance. This possibly explains why the TEs of many ISGs are generally low (Fig. 2b).

Mature tRNAome regulates the antiviral potency of IFN-α by enabling ISG translation.

Having discovered that tRNAome remodeling coordinates the TEs of ISGs, we further investigated whether tRNAome modulation affects the interferon antiviral response. HEV is a major cause of acute viral hepatitis in humans[44]. It belongs to the *Hepeviridae* family and is characterized by a single-stranded positive-sense RNA genome. A key step in tRNAome maturation involves the addition of CCA nucleotides to pre-tRNAs, which is exclusively executed by tRNA nucleotidyltransferase 1 (TRNT1) (Fig. 3a). Two previously validated small interfering RNAs (siRNAs) from the Sigma-Aldrich library were used for the TRNT1 knockdown (Supplementary Table 2). By inhibiting this key step of tRNAome maturation, the assay can thus downregulate the levels of the mature tRNAome. The two

siRNAs reduced several mature tRNAs (Fig. 3b). Importantly, the knockdown of TRNT1 functionally lowers the anti-HEV effect of IFN-α (Fig. 3c). Following TRNT1 knockdown, mRNA levels of ISG15 and IFIT3 remain almost unchanged; however, the synthesis of ISG proteins, particularly ISG15, is dramatically reduced (Fig. 3d-e). This suggests that tRNAome maturation regulates the interferon antiviral effect through the ISG mRNA-tRNAome-protein axis. Because viral translation also relies on the host's tRNAome, we found that the synthesis of the HEV ORF2 protein is reduced upon TRNT1 knockdown (Fig. 3f).

After maturation, tRNAs require charging with their respective amino acids (AAs) to become functional. We subsequently tested whether the AA charging of the tRNAome affects the antiviral effect of IFN-α. An AA-reduced medium was employed while maintaining vitamins and buffering ions (referring to DMEM medium) to selectively inhibit tRNAome charging[16, 30, 45]. Upon limiting AAs to 25% of normal levels, the levels of many non-charged tRNAs were increased (Fig. 3g, Supplementary Fig.7a), and intracellular AA-related metabolites were substantially reduced (Supplementary Fig. 7b). Without IFN-α treatment, HEV replication increased in the AA-limited cells (Supplementary Fig. 8a-b). Nonetheless, IFN-α retains its antiviral activity against HEV in the charging-inhibited cells (IFN-α treated versus untreated) (Fig. 3h). However, when compared to the cells cultured in media containing normal AA concentrations (100%), the anti-HEV effect of IFN-α is significantly reduced in the charging-inhibited cells (Fig. 3h). We also examined the impact of charging inhibition on the anti-HEV effect of IFN-α in both pre-treated and post-infection cells. In both scenarios, charging inhibition decreases the anti-HEV effect of IFN-α (Fig. 3i). In the IFN-α pretreated cells, HEV RNA loads are the highest at 8 h compared to 4 h or 24 h of pretreatment (Fig. 3i). Conversely, in post-infected cells, the changes in HEV RNA loads follow a different pattern, gradually decreasing over time (Fig. 3i). Interestingly, in the IFN-α pretreated groups, the increase in HEV RNA loads due to tRNAome charging inhibition is inversely correlated with the TE dynamics of core ISGs

(Fig. 2b). When the TEs of ISGs decrease or remain steady from 4h to 8h (Fig. 2b), the HEV RNA titers increase (8h vs. 4h) (Fig. 3i); in contrast, when their TEs increase (24h vs. 8h), the HEV RNA titers accordingly decrease. Furthermore, coinhibition of both tRNAome charging and maturation furthermore shrinks the anti-HEV effect of IFN-α (Fig. 3j), indicating that both tRNAome maturation and charging regulate the antiviral response to IFN-α.

When tRNAome charging inhibition is alleviated by supplementing all twenty AAs, intracellular AA- related metabolites increase (Supplementary Fig. 7b). Consequently, this results in approximately a 4-5-fold increase in the interferon effect against HEV RNA replication (Fig. 3k, Supplementary Fig. 8c). Mechanistically, AA-restricted cells show a sharp decrease in the protein synthesis of ISG15 and IFIT3, while their transcription remains largely unchanged (Fig. 3l-n). Recovery from AA limitation profoundly enhances ISG protein synthesis. Under these conditions, the integrated stress response (ISR) may be activated[46]. Nevertheless, we found that the ATF4 protein and phosphorylated eIF2α, markers of ISR, are controlled by tRNA charging inhibition and disinhibition, akin to ISG protein synthesis (Fig. 3m-n), with their mRNA levels also remaining unaffected (Fig. 3l). Additionally, supplementing each AA partially rescues the anti-HEV effect of IFN-α (Fig. 3o). Since both host and viral mRNAs rely on the same cellular tRNA pool. As observed, blocking tRNA maturation and charging also led to a decrease in HEV protein expression (Fig. 3f and 3p), in addition to ISG's translation (Fig. 3m-n). Taken together, our results indicate that the mature tRNAome regulates the antiviral potency of IFN-α by enabling ISG protein translation, while viral protein synthesis is simultaneously constrained by the same tRNA-dependent translational capacity.

DHBV and HBV infections differently remodel the host tRNAome while sparing the ISG response.

Unlike many other viruses, HBV infection does not induce an ISG response[26, 47]. In this regard, the mature tRNAome, when remodeled by HBV infection, could instead promote

HBV replication. Mammalian HBV and avian HBV (with the prototype being duck HBV [48]) are hepatotropic DNA viruses belonging to the *Hepadnaviridae* family. The Huh7 cells lack the human HBV receptor and are, therefore, not susceptible to direct infection; however, duck HBV (DHBV) can naturally infect human Huh7 cells[49]. Exploiting the DHBV infection model, a well-recognized proxy for studying HBV infection[49], we confirmed DHBV infection in the human hepatocytes (Fig. 4a-c) and in duck primary hepatocytes (DPHs) (Fig. 4d-f). In human hepatocytes, DHBV infection led to a gradual increase in intracellular DHBV DNA (Fig. 4a), pgRNA transcripts (Fig. 4b), and viral release into the medium (Fig. 4c). In duck hepatocytes, DHBV replication and release, as well as active pgRNA transcription, were also observed (Fig. 4d-f). Additionally, DHBV infection in human cells was confirmed by the expression of its core protein (Fig. 4g). Interestingly, DHBV infection in both human and duck hepatocytes induced a remodeling of the mature tRNAome (Fig. 4h-i), and human HBV infection also remodeled the tRNAome in HepG2-NTCP (Na+-taurocholate cotransporting polypeptide (NTCP, HBV receptor) cells (Supplementary Fig. 9a-b). Compared to the DHBV duck cell model, the remodeling induced by human HBV in NTCP cells is less robust (Supplementary Fig. 9a-b). This suggests that while both DHBV and HBV regulate host tRNAome, the remodeling of tRNAome is host- and virus-specific.

Consistent with previous investigations[26, 47], the host ISG responses in human and duck hepatocytes infected with DHBV or HBV were indeed not induced (Fig. 4j-o). In DHBV-Huh7 cells, the expression of ISG15, STAT1, and IFIT3 proteins, as well as their transcriptional activation (Fig. 4j-k) were not observed, nor was the induction of other ISGs (Fig. 4l-m). In human HBV infected NTCP stably expressed hepatocytes, the findings were largely the same, with negligible ISG transcription, signaling, or minimal ISG protein expression (Fig. 4n-o).

Since codon similarity between a virus and its paired host correlates with viral translation[50], it is likely that human HBV adapts to the codon patterns of its host. To

explore this, we performed a codon usage bias (CUB) analysis of the HBV surface (S) protein, polymerase (P), core (C) protein and the X gene, and found that these genes exhibit distinct patterns (Supplementary Fig. 10a). We then analyzed the relative synonymous codon usage (RSCU) of these four HBV genes against those of their human host. Interestingly, the four genes showed varying degrees of adaptation to human codons (Supplementary Fig. 10b). Surprisingly, the core protein gene exhibited no adaptation to human codons (R = 0.01) (Supplementary Fig. 10b). Our results suggest that, rather than relying on an adaptation to its host codons, the remodeled tRNAome, authentically employed for viral translation, should profit HBV infection. However, this possibility remains largely unexplored.

tRNA-Arg-UCU is a prominent tRNA that correlates with high AGA decoding of the HBV core protein gene.

To identify key proviral tRNAs, we conducted an association analysis between tRNAome availability and the codon usage bias (CUB) of DHBV. The DHBV genes encoding the C, P, and S proteins (n = 67) and human and duck CDS (n = 93,487 and 151, respectively) were plotted against the virus-remodeled tRNAome data. Among all pairs, our analysis revealed a particularly strong association between the duck tRNA-Arg-UCU isodecoder and the DHBV core protein gene (Supplementary Fig. 10c-d). The tRNA-Arg-UCU decodes the AGA codon. Consistently, the DHBV core gene contains the highest proportion of AGA codons within the arginine family (Supplementary Fig. 10e). Notably, the HBV core gene has not adapted to its human host (Supplementary Fig. 10b). These analyses suggest the notion that the host tRNAome, especially the upregulated tRNA-Arg-UCU, may promote HBV infection. Unlike in DHBV-preferring duck cells, the levels of human tRNA-Arg-UCU are not altered during DHBV infection (Supplementary Fig. 10f-g). This species-specific remodeling of tRNA-Arg-UCU may reflect the varying fitness of DHBV in human versus duck cells (Fig. 4a-f).

Overexpression of tRNA-Arg-UCU enhances DHBV protein synthesis and DNA replication.

In humans and ducks, there are five and three loci that encode different tRNA-Arg-TCT genes, respectively. Interestingly, paired sequence alignment showed that all three duck loci are identical to their human counterparts (Fig. 5a). To identify which tRNA gene predominantly promotes DHBV infection, we performed overexpression experiments. Each tRNA-Arg-TCT gene was cloned into a lentiviral plasmid containing two identical tRNA genes driven by the U6 promoter[28] (Supplementary Table 3). All five tRNA-Arg-TCT genes were successfully transduced, exhibiting varying levels of upregulation (at least a two-fold increase) (Fig. 5b). Among them, the overexpression of tRNA-Arg-TCT 1-1, although not the highest one, strongly enhanced DHBV DNA replication (Fig. 5c). Importantly, overexpression of this tRNA leads to a substantial increase in viral core protein synthesis as shown by blotting analysis (Fig. 5d) and IFA assay (Supplementary Fig. 11a), while the effects of the other tRNAs are relatively mild. Similarly, in duck hepatocytes, transfection of the three identical tRNA-Arg-TCT genes resulted in roughly a 2~5-fold upregulation (Fig. 5e). Furthermore, tRNA-Arg-TCT 1-1 boosts DHBV DNA replication in infected duck cells (Fig. 5f), and promotes core protein synthesis (Fig. 5g, Supplementary Fig. 11b). Our analysis confirms the importance of tRNA-Arg-UCU in DHBV DNA replication, while its decoding advantage for core protein synthesis is fundamental.

Interference with tRNA-Arg-UCU inhibits DHBV DNA replication and core protein synthesis.

Mature tRNAs exist in two states: AA-charged and uncharged (Fig. 6a). We employed an arginine-free culturing to inhibit the charging of tRNA-arginine while supplementing with a cocktail of the other 19 AAs[30, 51]. In human hepatocytes, arginine depletion resulted in an increase in uncharged tRNA-Arg-UCU levels (Fig. 6b). Consequently, inhibiting tRNA-Arg-UCU charging reduced DHBV DNA replication, while adding back the arginine

increased replication (Fig. 6c). These assays were repeated in duck hepatocytes (Fig. 6d-e), corroborating that the charging of tRNA-Arg-UCU regulates DHBV replication.

tRNA decoding relies on the accurate reading of codons within mRNAs. Errors in this step are defined as misdecoding, a process involving the incorrect interpretation of codons into the wrong AAs[14]. The charging of tRNA-Ala acceptors relies on the G3:U70 base pair, rather than on its anticodon[52]. Following our recent study[32], we constructed a "tRNAm-Ala-UCU" mutant, which harbors a backbone from one tRNA-Ala isoacceptor and an Arg-UCU anticodon. Using lentiviral vectors, we transduced the tRNA-Arg-UCU 1-1, tRNAm-Ala-UCU, and a non-cognate tRNA-Ser-UGA into Huh7 cells. All three selected clones showed upregulation of their respective tRNA species (Fig. 6f). As tested, the wild-type tRNA-Arg-UCU increased intracellular DHBV DNA levels, while other two tRNAs were less effective (Fig. 6g). Importantly, the effects of these tRNAs on DHBV DNA replication correlated with their impact on viral core protein synthesis (Fig. 6h, i). Additionally, these results observed in human cells were confirmed in the infected duck hepatocytes (Fig. 6j), where parallel impacts on viral DNA replication (Fig. 6k) and core protein synthesis (Fig. 6l, m) were observed.

The decoding advantage of tRNA-Arg-UCU relies on the presence of AGA codons in the DHBV core protein gene.

Next, we examined the decoding dependence between tRNA-Arg-UCU and the AGA codons of the HBV core gene, creating an AGA>AGG mutant by replacing all AGA codons with synonymous AGG codons (Supplementary Table 4). This mutant alters the nucleotide sequence while preserving the protein sequence the same as the wild type (Fig. 7a). We investigated the impact of the AGA>AGG mutant on the TE of the core protein, assessing its effects while overexpressing the wild type tRNA-Arg-UCU in both hepatocytes (Fig. 7b, c). In human hepatocytes, the AGA>AGG mutation almost diminishes core protein synthesis (Fig. 7b). A similar result was observed in duck hepatocytes (Fig. 7c). In contrast, the wild-type core protein gene is efficiently expressed

in both cell types, with its expression further enhanced by tRNA-Arg-UCU overexpression (Fig. 7b, c). These findings confirm that the decoding advantage of tRNA-Arg-UCU specifically acts on AGA codons within the core protein gene. Interestingly, both viral core protein synthesis and DNA replication are promoted by this tRNA (Figs. 7b-c and 5c). This interested us to investigate how tRNA-Arg-UCU links HBV DNA replication and core protein synthesis [53].

tRNA-Arg-UCU additionally affects DHBV pgRNA transcription.

HBV genomic replication specifically begins with the packaging of pgRNA, which undergoes reverse transcription (RT) to produce rcDNA and eventually covalently closed circular DNA (cccDNA); while the pgRNA also serves as an mRNA template for core protein synthesis[53] (Fig. 7d). Notably, HBV DNA replication specifically occurs inside the nucleocapsid[53], which consists of core proteins. The core protein contains an assembly domain and an arginine-rich domain for pgRNA packaging (Fig. 7e). When the rcDNA inside is converted into cccDNA, it becomes a new template for pgRNA transcription, with the new pgRNA being translated or packaged for replication again[53, 54].

Considering the vital role of tRNA-Arg-UCU in HBV core protein synthesis and DNA replication, as well as the indispensable role of pgRNA within, we investigated whether tRNA-Arg-UCU also additionally affects pgRNA transcription (Fig. 7d). Interestingly, among all isodecoders the tRNA-Arg-UCU 1-1 strongly activates pgRNA transcription in both hepatocytes infected with DHBV (Fig. 7f, g). The specificity of tRNA-Arg-UCU 1-1 was further validated by a comparison with a non-cognate tRNA-Ser-UGA in both human and duck cells (Fig. 7h, i). In contrast, arginine deprivation, which inhibits tRNA-Arg-UCU charging, suppressed pgRNA transcription in human and duck hepatocytes (Fig. 7j, k) and this can be reversed by adding the arginine back.

These findings suggest that while tRNA-Arg-UCU primarily supports HBV core protein synthesis and DNA replication, it also plays a secondary, yet significant, role in pgRNA transcription. This contrasts with the role of the tRNAome in the interferon

response, where interference with the tRNAome spares the transcription of ISGs (Fig. 3l, Supplementary Fig. 12a), although it does inhibit protein synthesis in general (Supplementary Fig. 12b) and ISGs specifically (Fig. 3m, n). Because ISG transcription occurs inside the nucleus, where the tRNAome does not function. However, HBV transcription and replication are influenced by core protein synthesis, which is regulated by host tRNAs.

Validation of tRNA-Arg-UCU in human HBV HepG-NTCP cells and Alb-Cre transgenic mice.

Using HepG2-NTCP cells, we tested whether overexpressing the tRNA-Arg-UCU promotes human HBV infection, at 5 dpi prior to reaching the viral infection peak, as reported[55]. Similarly, we found that tRNA-Arg-UCU significantly increases human HBV DNA replication, pgRNA transcription (Fig. 8a), and core protein expression (Fig. 8b). Given that this tRNA affects HBV pgRNA transcription and replication, we then examined whether blocking HBV DNA synthesis with Entecavir (ETV) would separate the effect of tRNA on pgRNA transcription from its influence on viral DNA replication. Although ETV primarily inhibits HBV DNA replication, it takes a longer period. After 21 days of ETV treatment, intracellular cccDNA levels were not inhibited as reported [55]. Following two days of concurrent ETV treatment and tRNA-Arg-UCU transduction, the inhibitory effect of ETV on HBV DNA levels was not evident (Fig. 8c). However, pgRNA transcription was significantly suppressed by 32.9%. Since ETV only inhibits the synthesis of new cccDNA while leaving the established largely unaffected[55], implying that there is likely a stronger pgRNA transcription from newly formed cccDNA over preexisting cccDNA.

In the HBV mouse model, the proviral role of tRNA-Arg-UCU was further confirmed. After 5 weeks of HBV infection, mice with similar HBV blood titers were intravenously administered 50 μL of 1.0×10^9 copies of lentiviruses containing either tRNA-Arg-UCU 1-1 or a scramble vector (Fig. 8d). Notably, the mouse genome transcribes the same tRNA-Arg-UCU 1-1 in sequence as it encoded in humans and ducks[56]. After 1 week, compared

to control groups more severe liver injuries were observed in HBV-infected mice undergoing transduction with tRNA-Arg-UCU 1-1 (Fig. 8e), with elevations in ALT and AST levels in blood tests, although not significant for AST (Fig. 8f). Importantly, transduction with tRNA-Arg-UCU 1-1 significantly promoted HBV DNA replication in liver tissues (Fig. 8h), and was accompanied by much higher core protein expression (Fig. 8g). Taken together, we conclude that host's mature tRNAome not only regulates the interferon response through the ISG transcriptome-tRNAome-proteome axis, but also actively promotes multiple stages of HBV infection especially when host antiviral responses are not activated (Fig. 9).

Discussion

The mature tRNAome, encompassing its abundance, processing, and modifications, has been linked to a host of diseases, particularly developmental disorders[29], cancer development[16, 27], and inflammatory responses[30]. These studies underscore the canonical role of the tRNAome; however, its regulatory roles in the virus-host battle race are uniquely dichotomous. Viruses, which are entirely dependent on the host tRNAome for protein production[13, 14, 17, 32, 33, 57], compete with the host's interferon-mediated antiviral response[3, 10], which relies on the same tRNA pool to orchestrate the ISG response and to fight for dominance in the race. This competition positions the tRNAome as a likely key regulator governing the infection outcome. Here, we bridge a knowledge gap: the mature tRNAome acts as a bidirectional "decoding switch", coordinating both the interferon response and HBV infection. To our knowledge, this is the first demonstration of such duality in the host mature tRNAome, joining previously transcript or protein-centric views of virus-host interaction.

The interferon response depends on the mature tRNAome to mount an integrated antiviral defense. Nevertheless, clinical observations have revealed that not all patients respond effectively to IFN-α therapy; only 20-40% of HBV patients respond well[21]. Similarly, chronic HEV infections sometimes show IFN non-responsiveness, suggesting

that either viral or host mechanisms may bypass or interfere with tRNAome-dependent ISG protein translation[58]. As reported, ISG transcriptomic signatures alone poorly predict clinical outcomes [36]. This observation aligns well with our findings: IFN-α-induced proteomic changes were highly disproportionate to their transcriptomic changes (Supplementary Fig. 2d). Importantly, we further demonstrate that IFN-α remodels the host mature tRNAome (Fig. 2c), dynamically fine-tuning the TEs of ISGs (Fig. 2b, j), which functionally affects the resulting anti-HEV efficacy of IFN-α (Fig. 3). This supports our hypothesis that the host mature tRNAome acts as a rheostat for IFN-α antiviral activity, and its dysregulation may correlate with clinical issues of non-responsiveness. Notably, restoring tRNAome charging results in a nearly 4-fold boost to the anti-HEV activity of interferon (Fig. 3k) which exceeds established inhibitory efficiencies[59, 60], implying a prominent role for the tRNAome in the interferon response.

It is well-known that mRNAs (including ISGs) and tRNAs are respectively transcribed by Pol II[3] and Pol III[20]. Our data show that when ISG transcription is most active (Fig. 1c), there is an accompanying downregulation of the mature tRNAome (Fig. 2c-e) and its transcriptional activity (Fig. 2l). This inverse relationship suggests a potential transcriptional competition or interference between Pol II and Pol III, a phenomenon previously described in human cells[39] where Pol II depletion can lead to an increased Pol III occupancy. While our current findings provide a correlative framework for this transcriptional competition, future studies utilizing a direct Pol II inhibition assay would definitively confirm this leading explanation.

Conversely, viral infection can remodel the host tRNAome to optimize their own infection. Because viral codons often differ from those of their host[50], necessitating host tRNAome adaptations to meet the translational demands of the invading viruses[13, 17, 20, 57]. While debates persist regarding viral-host codon similarity[61] versus dissimilarity[50], both viral and host mRNAs ultimately depend on the same tRNA pool for decoding, with decoding efficiency dictated by codon context and tRNA abundance[42]. As stated by the

translation hypothesis[1, 42], frequent use of a viral codon should correlate with elevated levels of its cognate tRNA to maximize TE[13]. Supportively, upregulation of tRNA-Ser-UGA which pairs with high UCA codons used in another duck hepatitis virus, promotes the viral translational decoding and its rapid dissemination[32]. Here, we extend this paradigm to HBV (especially DHBV) infection, which does not activate ISG signaling, and find that (D)HBV actively remodels the host tRNAome. Interestingly, the cross-species identical tRNA-Arg-UCU can be robustly remodeled in naturally DHBV-infected duck hepatocytes, and functionally promotes human HBV infection both *in vitro* and *in vivo*. Our observations underscore tRNAome remodeling as a likely common viral strategy to overcome host-virus codon dissimilarity and dominate host AA nutrients for viral translational decoding, thereby infection advantage.

Given that HBV core proteins are vital for viral DNA replication[53], this has spurred the development of a class of antivirals known as capsid assembly modulators (CAMs)[62, 63]. CAMs disrupt nucleocapsid formation by either misdirecting nonfunctional capsids or promoting the assembly of empty capsids, thereby blocking viral replication[62, 63, 64, 65]. Coincidentally, the tRNA-Arg-UCU that we discovered also highlights its important role in HBV infection, implying another potential anti-HBV target: this tRNA drives *de novo* core protein synthesis, and additionally affects multiple stages of HBV infection. Combining approaches that concurrently inhibit core protein *de novo* synthesis and later capsid assembly may lead to more dramatic inhibition of HBV replication. Despite this important potential, when host antiviral immunity is suppressed or evaded[26], the virus can modulate the host tRNAome to fuel infection.

In summary, we demonstrated that the mature tRNAome acts as a dual regulator in virus-host interactions. As we independently investigated the tRNAome's roles in the IFN-α response and HBV infection, future work should address how individual infected cells partition tRNA resources to balance competitive antiviral and proviral responses[5, 6]. While tRNA availability regulates the translation of both host antiviral and viral genes, this

mechanism likely coordinates with other interferon- or virus-induced translational controls, such as PKR-mediated eIF2α phosphorylation, mTOR signaling, and IFIT-mediated translational selection[1, 45]. These discoveries enhance our understanding of tRNAome remodeling in virus-host interactions and may inspire the development of tRNA-based strategies in translational medicine.

Methods

Ethical statement and animal housing

The mouse study was reviewed and approved by the Animal Welfare Committee, Sichuan Agricultural University (Protocol No. SYXK2025-112). All experimental work related to human HBV was conducted in a BSL-2 facility. Mice were housed in individually ventilated cages with wood shavings. The animals were maintained on a 12-h light/12-h dark cycle at a constant ambient temperature and a relative humidity of 50 ± 10%. All mice had *ad libitum* access to a standard pellet diet and sterilized water.

Cell culture and reagents

Duck hepatocytes were obtained from the liver of sixteen-day-old duck embryos and prepared following our previous publications[31]. The HCC cell line Huh7 and HepG2-NTCP[66] were cultured in DMEM with 10% fetal bovine serum, penicillin (100 units/mL), and streptomycin (100 μg/mL) at 37°C in a 5% CO_2 atmosphere, with the NTCP stable HepG2 cell line supplemented with 500 μg/mL G-418 (Geneticin). Entecavir (MCE, HY-13623), Cycloheximide (MCE, HY-12320), and G-418 (MCE, HY-108718) were purchased from MCE company. IFN-α 2b (Cat#, 540222) and puromycin (Cat#, P9620) were purchased from Sigma-Aldrich company.

Viruses

A plasmid construct containing the full-length genotype 3 HEV genome (GenBank: JQ679013) was transcribed into genomic RNA using the mMessage mMachine T7 RNA kit (Invitrogen)[44]. The viral RNA was transfected into cells to produce infectious HEV virions, which were used for secondary infection of naïve cells to generate the virion stock. HepAD38 (HepG2 derivative) cells cultured in a tetracycline free medium were used to produce HBV virions, which were quantified by qPCR[67]. The DHBV SCP01 strain (GenBank: KM676220.1)[68], isolated from diseased ducks, was stored at the Sichuan Agricultural University. The DHBV virus stock was derived from the supernatants of DHBV-infected DPHs.

RNA isolation and qRT-PCR.

RNA was isolated using the RNAiso plus isolation kit from Takara Biotech (Takara, cat# 9108) and reverse-transcribed into cDNA using the PrimeScript™ RT Master Mix (Takara, cat# RR036A), following the manufacturer's instructions. mRNA quantification by qRT-PCR was performed using SYBR™ Green PCR Master Mix (Vazyme, Q712) in a Real-Time PCR System (Bio-Red CFX96). Primer sequences targeting human and duck ISGs are provided in Supplementary Tables 5-6.

Mature tRNAome quantification

Human and duck mature tRNAomes were quantified following previous papers[17 31]. When the total RNA was not treated by the deacylation reaction, in which only the uncharged tRNAs could be ligated with the hybrid adaptor. This modification enables the quantification of un-charged tRNA levels, which has been applied in human cells[32, 45]. Primers used for tRNAome quantification were provided in Supplementary Tables 7-8.

RNA seq

Total RNA was extracted using the RNA Isolation Kit (Ambion) following the manufacturer's protocol. Libraries were constructed using the TruSeq Stranded mRNA LTSample Prep Kit (Illumina, San Diego, CA, USA) according to the manufacturer's instructions. These libraries were sequenced on the Illumina sequencing platform (Illumina HiSeq X Ten), and 125bp/150bp paired-end reads were generated.

Quantitively proteomic mass spectrum

TMTpro 16-plex mass spectrometry was performed on samples matched with RNA-seq data; detailed experimental design can be referenced in Supplementary Fig. 2. Lyophilized samples were resuspended in 100 μL of 100 mM TEAB (pH 8.5), and 40 μL of each sample was labeled. Ten microliters of TMTpro labeling reagent (ThermoFisher) were added to each sample, followed by 5 μL of 5% hydroxylamine to quench the reaction, which was then incubated for 15 minutes. Mass spectrometric analysis was performed using a Q-Exactive HF mass spectrometer with a Nanospray Flex source. Peptides were separated by a C18 column (15 cm × 75 μm) on an EASY-nLCTM 1200 system, using a 75 min gradient. Full MS scans were acquired from 350-1500 m/z with a resolution of 60,000, and the 20 most intense peaks were fragmented by HCD (collision energy of 32). MS/MS spectra were acquired at a resolution of 45,000.

Data analysis of ISG transcriptome and proteome

For the annotation of RNA sequencing reads, the human genome assembly GRCh38.p13 (hg38) was used. For peptide annotation from the TMTpro 16-plex experiment, the search database is uniprot-reviewed_yes+taxonomy_9606.fasta with the following parameters, such as static modification: TMT (N-term, K); carbamidomethyl(C); dynamic modification: oxidation(M), acetyl(N-term); digestion: trypsin; instrument: Q Exactive HF; MS1 tolerance:10 ppm; MS2 tolerance: 0.02 Da; and missed cleavages. Raw data from RNA-

seq were filtered using standard data processing methods. ISG candidates with their mRNA FC > 2 were selected for further analysis. The ISGs with their protein FC significantly higher than 1.2 were selected for subsequent analysis. The genome-wide IFN-α response at the mRNA and protein levels was summarized in Supplementary Table 1.

Ribosome profiling

The samples were pretreated with cycloheximide (50mg/mL) and lysis buffer, and endoribonuclease RNase I to digest ribosome unprotected fragments. Monosomes were acquired by size-exclusion chromatography with MicroSpin S-400 HR columns. Following PAGE purification, the both ends of the ribosome profiling fragments (RPF) were phosphorylated and ligated with 5' and 3' adapters respectively. To deplete rRNA contamination, the RNA samples were then treated with an rRNA depletion kit (Qiagen, 334387). The fragments were subsequently reverse transcribed into cDNAs. After PCR amplification, the samples were subjected to Illumina sequencing using SE50 (single-end 50nt) sequencing. Raw data (raw reads) in FASTQ format were processed to remove low quality reads. RNA-seq was performed simultaneously to calculate the TE of genome-wide ISGs, which refers to how often that mRNA binds to ribosomes, calculated as TE = (RPKM in Ribo Profiling)/(RPKM in RNA-seq).

tRNA transcription reporter assay

To investigate the impact of IFN-α on tRNA transcription, a tRNA transcription reporter plasmid was constructed (Supplementary Fig. 4). This reporter exploited an upstream sequence of tRNA-His-GTG which contains a key element (i.e., the TATA box) for binding type II RNA polymerase III (also known as tRNA specific RNA pol III). This sequence follows a tRNA-Met-CAU sequence. Additionally, we added another 44 nt of random sequence to extend the length of the tRNA reporter-derived transcripts, which benefit

qRT-PCR quantification while avoiding interference from cell-derived tRNA transcripts. tRNA transcription activity was quantified using the tRNA-Met-CAU binding primer (5'CTCGGTGGCTCAGTGGTTAGAG3', forward) and the random sequence binding primer (5'AGTGATATCACCGGTATATTACTACTGCCC3', reverse).

TRNT1 and SLFN11 knockdown

Two TRNT1-targeting siRNAs, synthesized by GenePharma, were used for the knockdown assay (Supplementary Table 2). The effect of TRNT1 knockdown was confirmed at a siRNA concentration of 30 pm/well in a 12-well plate. After 12 hours of transfection, the efficiency of tRNAome maturation inhibition was evaluated by quantifying the levels of several mature tRNAs[17]. SLFN11 knockdown was performed by transfecting the cells with three siRNAs (40 pm/well, GenePharma). The impact of SLFN11-knockdown on IFN-α-mediated tRNA remodeling (1000 IU/mL) was investigated and compared with the control groups transfected with NC-siRNAs.

Metabolomic profiling

Hepatocytes cultured in normal medium, AA poor medium (i.e., 25% of normal medium) and AA poor-to-normal medium were separately treated with 8h of IFN-α at a concentration of 1000 IU/mL (n = 6). Normal cultured cells without IFN-α served as controls. All samples were processed according to standard procedures. Metabolomic profiling was performed using an ACQUITY UPLC I-Class Plus coupled with a Q Exactive mass spectrometer. Chromatographic separation was achieved on an ACQUITY UPLC HSS T3 column (100 mm × 2.1 mm, 1.8 μm, 45°C) with a gradient of 0.1% formic acid (A) and acetonitrile (B) at 0.35 mL/min. The original LC-MS data were processed by Progenesis QI V2.3 software (Nonlinear, Dynamics, Newcastle, UK). The main parameters of 5 ppm precursor tolerance, 10 ppm product tolerance, and 5% product ion threshold were applied. Compound identification was based on the precise mass-to-

charge ratio (M/z), secondary fragments, and isotopic distribution using databases such as the Human Metabolome Database (HMDB), Lipidmaps (V2.3), Metlin, EMDB, PMDB, and self-built databases for qualitative analysis. Differential metabolites were selected based on VIP values greater than 1.0 and p-values less than 0.05.

Amino acid deprivation assays

According to a previous method[16, 45], charging inhibition assays were achieved by partially reducing the concentration of the twenty AAs in DMEM medium to 25% of the normal level. This was specifically done by diluting normal DMEM medium with HANK solution (Sigma-Aldrich, cat# H9269) and a glucose and MEM vitamin solution (100×) (Sigma-Aldrich, cat# M6895). Cells were harvested for non-charging tRNA quantification. The tRNAs were not treated with deacylation buffer and only the AA-free tRNA could be ligated to the adaptor for later PCR quantification.

Puromycin-labelling polypeptide assay

To label elongating polypeptides, the culturing medium containing 3 μg/mL of puromycin was preincubated for 30 min before sample collection. These cells were then analyzed by an IFA assay. Following the standard protocol, the slides were incubated with primary mouse anti-puromycin antibody (1:8000) overnight at 4 ℃ (Merck, Cat.: MABE343). The Alexa Fluor 594-conjugated goat anti-mouse IgG secondary antibody was then further incubated for 1.5 h. Nuclei were stained with DAPI. The slides were imaged and analyzed using image J software.

HBV infection in human and duck hepatocytes

For human HBV infection in HepG2-NTCP cells [66], the TaKaRa MiniBEST Universal Genomic DNA Extraction Kit Ver.5.0 (Cat#, 9765) was used to isolate DNA during revision, specifically treating the sample with proteinase K to remove viral polymerase and

removing RNA by treating the nucleic acid with RNase A. For duck HBV infection assays, DNAiso (Takara, cat# 9770A) was used as the samples treated or not treated with proteinase K did not significantly affect the quantification[48]. DPHs or human hepatocytes were seeded in a 12-well plate and allowed to grow until reaching ~60% confluence before inoculating with DHBV, 1×10^8 copies per well. After 24 or 48 hpi, 500 μl of lysis buffer was added to lyse the cells, and both cell lysates and supernatants were used for DNA extraction to quantify viral DNA levels.

Quantification of ISG transcription upon HBV and DHBV infections

DHBV was inoculated into human and duck hepatocytes, as well as HBV in HepG2-NTCP cells following previous publications[66]. At the indicated times, RNA samples were collected to assess the changes in ISG gene expression. Total RNA from the human or duck liver cells was extracted using the RNAiso Plus Reagent (Takara, cat# 9108), and followed by cDNA synthesis. Subsequently, RT-qPCR was conducted using the Taq Pro Universal SYBR qPCR Master Mix (Vazyme, Q712) according to the manufacture's protocol. The human and duck ISG primers are listed in Supplementary Tables 5-6.

Codon usage and tRNA abundance association analysis

The codon usage of humans and ducks was downloaded from the codon usage database and repurposed for this study. The codon usage bias of human ISGs and HBV (human and duck isolates) was analyzed using Codon W software (version 1.4.2) with standard genetic codes. The genome sequence of DHBV was downloaded from NCBI GenBank. The relative fold changes of each tRNA species in corresponding duck or human hepatocytes were normalized to the uninfected control groups. The codon usage index, RSCU, used by DHBV, humans and ducks, was correlated with the changes in the tRNAs according to the base pairing rule between tRNA anticodons and codons. The association

analysis between codon usage bias and tRNAome data was analyzed and visualized using Python Matplot and Seaborn tools.

Arginine deprivation and rescue assay

Arginine deprivation medium was prepared with Hank's balanced salt solution, glucose, and penicillin streptomycin solution. All AAs except for arginine were added according to the DMEM medium formulation. After pre-culturing for 48h in an arginine-depleting medium, the cells were infected with DHBV for additional 48h. The effects of arginine deprivation on DHBV DNA replication and pgRNA transcription were assessed by qPCR or RT-qPCR. For the arginine rescue assay, after culturing cells in the arginine-deficient medium for 48 h, we replaced the medium with an arginine containing medium and incubated for an additional 12 h. Subsequently, the cells were infected with DHBV and continually cultured in an arginine containing medium. After 48 hpi, the samples were collected, and intracellular DNA and RNA were separately extracted for DHBV DNA and pgRNA quantification.

Lentiviral tRNA packaging and transduction

The plko.1 plasmids inserting different tRNA sequences were constructed and sequenced. When 293T cells reached 80% confluence, the lentiviral packaging plasmids (VSVG, REV, MD) and the various plko.1-tRNA expression vectors (Supplementary Table 3) were separately transfected into 293T cells using PEI according to the standard protocol. The lentivirus-containing mediums expressing different tRNA-Arg-UCU isodecoders were used to incubate human hepatocytes. After 48 h, these cell lines were treated with 3 ug/mL of puromycin to obtain tRNA-stable expression cell lines. These cell lines were then inoculated with 1×10^8 copies per well of DHBV. Two micrograms of the duck tRNA expression plasmids were transfected into DPHs. After 12 h of transfection, we replaced the medium and inoculated 1×10^8 copies per well of DHBV. After 24 hpi, samples were

collected for quantifying DHBV DNA replication.

Immunoblotting

The protein expression levels of ISG15, IFIT3, STAT1, STAT1-pi (Tyr701), eIF2α-pi, ATF4, and SLFN11 under different conditions were analyzed by immunoblotting following standard protocols. The following antibodies were purchased from Beyotime: anti-ISG15 (AF7305, 1:1000), anti-IFIT3 (AG2254, 1:1000), anti-STAT1 (AG3318, 1:1000), anti-STAT1-pi (Tyr701) (AF5935, 1:750), anti-ATF4 (AF2560, 1:1000), and anti-eIF2α-pi (Ser51) (AF1237, 1:1000). Additionally, HEV anti-ORF2 antibodies were purchased from Abcepta (Cat: AP56287, 1:1000). To assess the impact of different tRNA-Arg-UCU vectors on DHBV or human HBV core protein synthesis, these vectors were first transfected into either DPHs or human hepatocytes. Furthermore, tRNA-overexpressing human and duck hepatocytes were transfected with wild-type or codon-reassignment core protein plasmid containing a Flag tag. The primary antibody, anti-DYKDDDDK Antibody (Flag) (Smart Lifesciences, cat# SLAB0100, 1:1000), was incubated, followed by incubation with the secondary antibody, Goat anti-Mouse or anti-Rabbit IgG (H + L)-HRP Conjugate (1:3000 both) (Bio-Rad, cat# 1706515/6, 1:3000). The protein bands of interest were visualized via an enhanced chemiluminescence (ECL) chromogenic kit (Beyotime Biotechnology, cat# P0018AS). The images were scanned and captured using the ChemiDoc MP Imaging System (Bio-Rad, USA).

Immunofluorescence assay

The impact of different tRNA-Arg-UCU vectors on DHBV core protein synthesis was analyzed by an IFA assay. Slides were fixed overnight at 4°C with pre-cooled 4% formaldehyde. The cells were then washed with TPBS and were permeabilized with 0.3% Triton PBS at 4°C for 1 hour and blocked with 5% BSA-PBS at 37°C for 1 hour. The anti-DHBV core protein rabbit antibodies (1:200) or the anti-Flag antibody (cat# SLAB0100,

1:400) were used as the primary antibodies. For core protein expression of HBV in human cells, a rabbit anti-HBcAg polyclonal antibody (Bioss Antibodies, cat# bs-15455R, 1:300) was used. The secondary antibodies used were Goat anti-Mouse IgG (H+L) Alexa Fluor™ Plus 488 (Thermo Scientific™, cat# A11034, 1:400) or YSFluor® 488 Goat Anti-Rabbit IgG, cat# 33106ES60, 1:400). The nucleus was stained with DAPI and sealed with a PBS-glycerol solution. Representative images were captured using a fluorescence microscope (BX53, OLYMPUS).

HBV transgenic mouse model

Recombinant adenoviral vectors were generated by constructing a pShuttle plasmid inserting a full length of HBV genome (subtype ayw; GenBank: V01460.1)[69]. The fragments were transferred to the E1 and E3-deleted pAdHu5 plasmid and transfected into HEK293 cells, resulting in purified and quantified adenoviruses. Alb-Cre Tg mice (C57BL/6-Tg 21Mgn/J), which express $Cre^{+/-}$ recombinase under the albumin promoter were intravenously administered by 1.5×10^9 plaque forming units (PFU) of adenoviral vectors. All mice were heterozygous males, aged 6-8 weeks. After 5 weeks, mice with HBV blood titers of approximately 1.0×10^4 per mL were randomly allocated into two groups and intravenously administered 100 µL of lentivirus containing 1.0×10^9 copies of either tRNA-Arg-UCU 1-1 or a scrambled vector sequence. After 1 week, the liver tissues and blood samples were collected for the analysis of HBV core protein synthesis and DNA replication, blood tests for liver function, and HE staining.

Statistical analysis

Key experiments for DHBV study were independently performed in duck and human cells. At least three biological replicates and two technical replicates were consistently used. All data were plotted using GraphPad Prism 8.0.1(http://www.graphpad.com). Data are presented as mean ± standard deviation. The student's t-test was employed for statistical

analysis as indicated in figure legends, with exact p values. $P < 0.05$ was considered as a statistical significance.

Data availability

The RNA sequencing and ribosome profiling data generated in this study have been deposited in the NCBI Sequence Read Archive (SRA) under BioProject IDs PRJNA853533 [https://www.ncbi.nlm.nih.gov/sra?term=PRJNA853533] and PRJNA1393751 [https://www.ncbi.nlm.nih.gov/sra/?term=PRJNA1393751]. The raw Tandem Mass Tag (TMT) proteomics data have been deposited in the iProX repository (accession ID: IPX0004647000), which is also accessible via the Proteome X change Consortium (accession ID: PXD035057). The raw data of metabolic analysis can be accessed in the China National Center for Bioinformation via the link: https://ngdc.cncb.ac.cn/omix/select-edit/OMIX015907. The source data underlying figures and supplementary figures are provided as a Source Data file. A reporting summary for this article is available as a Supplementary Information file.

References

1. Rozman B, Fisher T, Stern-Ginossar N. Translation—A tug of war during viral infection. *Molecular cell* **83**, 481-495 (2023).
2. Ungerleider NA*, et al.* Viral reprogramming of host transcription initiation. *Nucleic Acids Research* **52**, 5016-5032 (2024).
3. Wang W, Xu L, Su J, Peppelenbosch MP, Pan Q. Transcriptional Regulation of Antiviral Interferon-Stimulated Genes. *Trends in Microbiology* **25**, 573-584 (2017).
4. Mostafavi S*, et al.* Parsing the Interferon Transcriptional Network and Its Disease Associations. *Cell* **164**, 564-578 (2016).
5. Kibe A*, et al.* The translational landscape of HIV-1 infected cells reveals key gene regulatory principles. *Nature Structural & Molecular Biology* **32**, 841-852 (2025).
6. Fulcher JM*, et al.* Parallel measurement of transcriptomes and proteomes from same single cells using nanodroplet splitting. *Nat Commun* **15**, 10614 (2024).
7. Toribio R, Ventoso I. Inhibition of host translation by virus infection in vivo. *Proceedings of the National Academy of Sciences* **107**, 9837-9842 (2010).
8. Li Y, Qu C, Yu P, Ou X, Pan Q, Wang W. The Interplay between Host Innate Immunity and Hepatitis

E Virus. *Viruses* **11**, 541-560 (2019).
9. Schneider WM, Chevillotte MD, Rice CM. Interferon-stimulated genes: a complex web of host defenses. *Annual review of immunology* **32**, 513-545 (2014).
10. Cheng J*, et al.* Interferon alpha induces multiple cellular proteins that coordinately suppress hepadnaviral covalently closed circular DNA transcription. *Journal of virology* **94**, e00442-00420 (2020).
11. Schoggins JW, Rice CM. Interferon-stimulated genes and their antiviral effector functions. *Current opinion in virology* **1**, 519-525 (2011).
12. Stadler D*, et al.* Interferon-induced degradation of the persistent hepatitis B virus cccDNA form depends on ISG20. *EMBO reports* **22**, e49568 (2021).
13. van Weringh A, Ragonnet-Cronin M, Pranckeviciene E, Pavon-Eternod M, Kleiman L, Xia X. HIV-1 modulates the tRNA pool to improve translation efficiency. *Mol Biol Evol* **28**, 1827-1834 (2011).
14. Ou X, Cao J, Cheng A, Peppelenbosch MP, Pan Q. Errors in translational decoding: tRNA wobbling or misincorporation? *Plos Genetics* **15**, e1008017 (2019).
15. Kwon NH, Fox PL, Kim S. Aminoacyl-tRNA synthetases as therapeutic targets. *Nature Reviews Drug Discovery* **18**, 629-650 (2019).
16. Zhang R*, et al.* The biological process of lysine-tRNA charging is therapeutically targetable in liver cancer. *Liver Int* **41**, 206-219 (2020).
17. Ou X*, et al.* A simplified qPCR method revealing tRNAome remodeling upon infection by genotype 3 hepatitis E virus. *FEBS Lett* **594**, 2005-2015 (2020).
18. Chan PP, Lowe TM. GtRNAdb: a database of transfer RNA genes detected in genomic sequence. *Nucleic Acids Res* **37**, D93-97 (2009).
19. Ou X*, et al.* Evolutionarily missing and conserved tRNA genes in human and avian. *Infect Genet Evol* **85**, 104460 (2020).
20. Dremel SE, Sivrich FL, Tucker JM, Glaunsinger BA, DeLuca NA. Manipulation of RNA polymerase III by Herpes Simplex Virus-1. *Nat Commun* **13**, 623 (2022).
21. Shen F*, et al.* Hepatitis B virus sensitivity to interferon-α in hepatocytes is more associated with cellular interferon response than with viral genotype. *Hepatology (Baltimore, Md)* **67**, 1237-1252 (2018).
22. Xu L*, et al.* RIG-I is a key antiviral interferon-stimulated gene against hepatitis E virus regardless of interferon production. *Hepatology (Baltimore, Md)* **65**, 1823-1839 (2017).
23. Wang W*, et al.* Unphosphorylated ISGF3 drives constitutive expression of interferon-stimulated genes to protect against viral infections. *Sci Signal* **10**, eaah4248 (2017).
24. Hsu Y-C, Huang DQ, Nguyen MH. Global burden of hepatitis B virus: current status, missed opportunities and a call for action. *Nature Reviews Gastroenterology & Hepatology* **20**, 524-537 (2023).
25. Miao Z*, et al.* Estimating the Global Prevalence, Disease Progression, and Clinical Outcome of Hepatitis Delta Virus Infection. *J Infect Dis* **221**, 1677-1687 (2020).
26. Suslov A, Boldanova T, Wang X, Wieland S, Heim MH. Hepatitis B Virus Does Not Interfere With Innate Immune Responses in the Human Liver. *Gastroenterology* **154**, 1778-1790 (2018).
27. Earnest-Noble LB*, et al.* Two isoleucyl tRNAs that decode synonymous codons divergently regulate

breast cancer metastatic growth by controlling translation of proliferation-regulating genes. *Nature Cancer* **3**, 1484-1497 (2022).

28. Wang J*, et al.* AAV-delivered suppressor tRNA overcomes a nonsense mutation in mice. *Nature* **604**, 343-348 (2022).
29. Gao L*, et al.* Selective gene expression maintains human tRNA anticodon pools during differentiation. *Nature Cell Biology* **26**, 100-112 (2024).
30. Li Y*, et al.* Hepatitis E virus infection remodels the mature tRNAome in macrophages to orchestrate NLRP3 inflammasome response. *PNAS* **120**, e2304445120 (2023).
31. Gong L*, et al.* Orchestration of hepatocyte inflammatory responses by monocytes during acute viral hepatitis in ducks in vitro. *Veterinary Research* **56**, 200 (2025).
32. Ou X*, et al.* tRNA-Ser-UGA efficiently promotes the rapid release of duck hepatitis A virus from infected enterocytes and its remote dissemination to hepatocytes. *Poultry Science* **104**, 104655 (2024).
33. Wang Y, Wang X, Avan A, Li P, Ou X, Pan Q. Coronaviruses remodel the mature human tRNAome to modulate infection. *Virulence* **16**, 2580129 (2025).
34. Wang W*, et al.* Convergent Transcription of Interferon-stimulated Genes by TNF-α and IFN-α Augments Antiviral Activity against HCV and HEV. *Scientific reports* **6**, 25482-25482 (2016).
35. Mergner J*, et al.* Mass-spectrometry-based draft of the Arabidopsis proteome. *Nature* **579**, 409-414 (2020).
36. Golden-Mason L, Rosen HR. Revisiting the Paradox of Interferon-Stimulated Gene Expression as a Predictor of Hepatitis C Virus Treatment Response, a Decade Later. *Hepatology (Baltimore, Md)* **68**, 2053-2055 (2018).
37. Hodge K, Makjaroen J, Robinson J, Khoomrung S, Pisitkun T. Deep Proteomic Deconvolution of Interferons and HBV Transfection Effects on a Hepatoblastoma Cell Line. *ACS Omega* **5**, 16796-16810 (2020).
38. Yu YC, Han JM, Kim S. Aminoacyl-tRNA synthetases and amino acid signaling. *Biochimica et Biophysica Acta -Molecular Cell Research* **1868**, 118889 (2021).
39. Gerber A, Ito K, Chu CS, Roeder RG. Gene-Specific Control of tRNA Expression by RNA Polymerase II. *Molecular cell* **78**, 765-778.e767 (2020).
40. Hou P, Hao W, Qin B, Li M, Zhao R, Cui S. Structural and biochemical characterization of Schlafen11 N-terminal domain. *Nucleic Acids Res* **51**, 7053-7070 (2023).
41. Dedon PC, Begley TJ. Dysfunctional tRNA reprogramming and codon-biased translation in cancer. *Trends Mol Med* **11**, 964-978 (2022).
42. Hernandez-Alias X, Benisty H, Schaefer MH, Serrano L. Translational adaptation of human viruses to the tissues they infect. *Cell Rep* **34**, 108872 (2021).
43. Horn D. Codon usage suggests that translational selection has a major impact on protein expression in trypanosomatids. *Bmc Genomics* **9**, 2 (2008).
44. Shukla P*, et al.* Adaptation of a genotype 3 hepatitis E virus to efficient growth in cell culture depends on an inserted human gene segment acquired by recombination. *Journal of virology* **86**, 5697-5707 (2012).
45. Ge M-K*, et al.* The tRNA-GCN2-FBXO22-axis-mediated mTOR ubiquitination senses amino acid

insufficiency. *Cell Metabolism* **35**, 2216-2230.e2218 (2023).
46. Labbé K*, et al.* Specific activation of the integrated stress response uncovers regulation of central carbon metabolism and lipid droplet biogenesis. *Nat Commun* **15**, 8301 (2024).
47. Mitra B*, et al.* Hepatitis B Virus Precore Protein p22 Inhibits Alpha Interferon Signaling by Blocking STAT Nuclear Translocation. *Journal of virology* **93**, 10.1128/jvi.00196-00119 (2019).
48. Lin X*, et al.* High prevalence of Duck Hepatitis B virus-associated coinfection in Southwest China. *PLOS ONE* **20**, e0324682 (2025).
49. Pugh J, Yaginuma K, Koike K, Summers. Duck hepatitis B virus (DHBV) particles produced by transient expression of DHBV DNA in a human hepatoma cell line are infectious in vitro. *Journal of virology* **62**, 3513-3516 (1988).
50. Chen F*, et al.* Dissimilation of synonymous codon usage bias in virus-host coevolution due to translational selection. *Nature ecology & evolution* **4**, 589-600 (2020).
51. Pavlova NN*, et al.* Translation in amino-acid-poor environments is limited by tRNAGln charging. *eLife* **9**, (2020).
52. Giegé R, Eriani G. The tRNA identity landscape for aminoacylation and beyond. *Nucleic Acids Research* **51**, 1528-1570 (2023).
53. Zhang T*, et al.* RNA binding protein TIAR modulates HBV replication by tipping the balance of pgRNA translation. *Signal Transduction and Targeted Therapy* **8**, 346 (2023).
54. Tsukuda S, Watashi K. Hepatitis B virus biology and life cycle. *Antiviral Res* **182**, 104925 (2020).
55. Ko C*, et al.* Hepatitis B virus genome recycling and de novo secondary infection events maintain stable cccDNA levels. *Journal of Hepatology* **69**, 1231-1241 (2018).
56. Chan PP, Lowe TM. GtRNAdb 2.0: an expanded database of transfer RNA genes identified in complete and draft genomes. *Nucleic Acids Res* **44**, D184-189 (2016).
57. Nunes A, Ribeiro DR, Marques M, Santos MAS, Ribeiro D, Soares AR. Emerging Roles of tRNAs in RNA Virus Infections. *Trends Biochem Sci* **45**, 794-805 (2020).
58. Dalton HR, Kamar N, Baylis SA, Moradpour D, Wedemeyer H, Negro F. EASL Clinical Practice Guidelines on hepatitis E virus infection. *Journal of Hepatology* **68**, 1256-1271 (2018).
59. Dong C*, et al.* Suppression of interferon-α signaling by hepatitis E virus. *Hepatology (Baltimore, Md)* **55**, 1324-1332 (2012).
60. Todt D*, et al.* Antiviral Activities of Different Interferon Types and Subtypes against Hepatitis E Virus Replication. *Antimicrobial agents and chemotherapy* **60**, 2132-2139 (2016).
61. Yu C*, et al.* Hepatitis B virus (HBV) codon adapts well to the gene expression profile of liver cancer: an evolutionary explanation for HBV's oncogenic role. *Journal of Microbiology* **60**, 1106-1112 (2022).
62. Nijampatnam B, Liotta DC. Recent advances in the development of HBV capsid assembly modulators. *Curr Opin Chem Biol* **50**, 73-79 (2019).
63. Lecoq L*, et al.* Molecular elucidation of drug-induced abnormal assemblies of the hepatitis B virus capsid protein by solid-state NMR. *Nat Commun* **14**, 471 (2023).
64. Pavlova A*, et al.* The Mechanism of Action of Hepatitis B Virus Capsid Assembly Modulators Can Be Predicted from Binding to Early Assembly Intermediates. *J Med Chem* **65**, 4854-4864 (2022).
65. Xi J*, et al.* A novel hepatitis B virus capsid assembly modulator QL-007 inhibits HBV replication and infection through altering capsid assembly. *Antivir Res* **218**, 105715 (2023).

66. Zhong G*, et al.* Sodium taurocholate cotransporting polypeptide is a functional receptor for human hepatitis B and D virus. *eLife* **1**, (2012).
67. Ladner SK*, et al.* Inducible expression of human hepatitis B virus (HBV) in stably transfected hepatoblastoma cells: a novel system for screening potential inhibitors of HBV replication. *Antimicrobial agents and chemotherapy* **41**, 1715-1720 (1997).
68. Li Q*, et al.* Complete genome sequence of the novel duck hepatitis B virus strain SCP01 from Sichuan Cherry Valley duck. *SpringerPlus* **5**, 1353 (2016).
69. Li G*, et al.* Recombinant covalently closed circular DNA of hepatitis B virus induces long-term viral persistence with chronic hepatitis in a mouse model. *Hepatology (Baltimore, Md)* **67**, 56-70 (2017).

Acknowledgements

This study was supported by the Sichuan Province Science and Technology Education Joint Fund Project (2025NSFSC2134 to XO), the Guizhou University Natural Sciences Project for Special Post (Leading Group 2024-12 to AC), the Hundred Thousand Million Leading Talent Teams of Guizhou Province (BQW2025-004 to AC), the Science and Technology Program of Sichuan Province (2020YJ0396 to XO), the NSFC (32102706 to XO), the Program Sichuan Veterinary Medicine and Drug Innovation Group of China Agricultural Research System (SCCXTD-2026-18 to MW), and the earmarked fund for China Agriculture Research System (CARS-42-17 to AC). The funders had no role in study design, data collection and analysis, decision to publish, or preparation of the manuscript. We thank Shanghai OE Biotech Co., Ltd., Tingjing Gong and Fengyuan Zhen for their technical support and bioinformatic analysis, and Siyu Zeng (Sichuan Agricultural University), Weixi Xie (Sichuan Agricultural University), Dr. Jibin Liu (Chengdu University of TCM), Dr. Qiupin Chen (Chengdu University of TCM), Peijie Wang and Yi Liu (Sichuan Agricultural University) for their help in preparing the reagents used in this study, as well as the mouse study.

Author contributions

X.O., Q.P., and A.C. conceived and designed the research; X.O., X.L., J.C., and W.Y. performed the experiments; D.S., S.C., M.L., D.Z., M.W., R.J., S.M., Y.W., and Q.Y. drafted the original manuscript and analyses the data; S.Z., X.Z., J.H., B.T., Z.W., and Y.H. conducted and analyzed RNA-seq and proteomics analysis; X.Z., J.H., X.O., and J.C. conducted and analyzed Ribo-seq assay; J.C. and X.L. respectively performed HEV related assays and DHBV study; X.O. X.L., and W.Y. performed the human HBV study *in vitro* and *in vivo*; X.O., Q.P., and A.C. wrote and revised the manuscript for important intellectual content.

Competing interests

The authors declare no competing interests.

Figure legends

Figure 1. **Dynamic changes in the ISG transcriptome and proteome upon IFN-α treatment. a** Illustration of the ISG gene-protein production line during the interferon response. The diagram demonstrates the bridging role of mature tRNAs in linking the ISG transcriptome to the proteome. **b** Heatmap showing dynamic changes in the genome-wide transcriptome following IFN-α (1000 IU/mL) treatment, based on three biological replicates. **c** Heatmap of changes specific to the ISG transcriptome. **d-e** Dynamic changes in global protein synthesis (d) and ISG proteome (e) with the same batches of cells treated by the same dose of IFN-α as panels b-c. Experimental design and technical details can be seen in materials and methods, and Supplementary Fig. 2. **f-h** Correlation analysis between the ISGs' mRNA FCs on the x-axis and corresponding protein FCs on the y-axis at 4h (f), 8h (g) and 24h (h). The FCs' datasets for ISG transcriptome and proteome were used, in which ISG candidates above either transcriptional (cutoff value, 2.0) or protein (cutoff value, 1.2) FC levels at least one time point were included. Statistical significance and correlation strength were determined using a two-sided Pearson's correlation coefficient (R) with linear regression analysis. For each comparison, the correlation coefficient (R) and p value are reported. All FC values were $\log_{10}$-transformed for normalization. **i-k** Time-point skewed correlation analyses of earlier mRNA FCs with later protein FCs: mRNA FCs at 4 h compared with protein FCs at 8 h (i), mRNA FCs at 8 h compared with protein FCs at 24 h (j), and mRNA FCs at 4 h compared with protein FCs at 24 h (k); datasets and statistical methods used are consistent with panels f-h. **l** Comparison analysis of ISGs responding at transcriptional levels (n =175) and protein levels (n = 36) at 4h, 8h, and 24h. Source data are provided as a Source Data file.

Figure 2. **IFN-α treatment remodels the mature tRNAome and affects translational efficiencies of ISGs. a** Genome-wide translational efficiencies (TEs), defined by the ratio of protein to mRNA fold changes (FCs), are presented for time points 4 h, 8h, and 24h of

IFN-α treatment (n = 4,191). A TE of 100% indicates a perfect match between protein and mRNA FCs; TEs below 100% correspond to decreased translational efficiency, with 572 genes exhibiting TEs less than 100% represented. **b** TEs for 36 core ISGs are plotted over time (4h, 8h, and 24h). **c** Heatmap illustrating changes in the mature tRNAome from 4h to 48h of IFN-α treatment (1,000 IU/mL, n = 3), normalized to untreated cells (set as 1.0). **d** Statistical analysis comparing mature tRNA levels across 4h, 8h, and 24h time points using a two-sided paired Student's t-test (n = 57 pairs, related to panel c). **e** Heatmap depicting the dynamics of the mature tRNAome with a lower concentration of IFN-α (10 IU/mL). **f** Proposed relationship between mature tRNAome availability and ISG TEs. **g** Changes in the transcription and protein abundance of tRNA-, translation, and ribosome-related genes (n = 244) based on human hallmark gene sets regulating protein translation. **h** Real-time analysis of potential ISGs identified through RNA sequencing (an independent RNA-seq) and ribosome profiling. **i** At 4h, 8h, and 24h, statistical analysis of abundance of ribosomes translating ISG mRNAs in rpkm using a two-sided student's t-test (n = 42 pairs). **j** Ribosome TE of core ISGs identified in panel b. **k** Design of a reporter plasmid for studying IFN-α's impact on tRNA transcription. **l** Cells transfected with the reporter plasmid show quantification of transcripts derived from the plasmid, reflecting the impact of IFN-α on tRNA transcription. Statistical analysis was performed using a two-sided student's t-test (n = 3 biological replicates). **m** Knockdown efficiencies of cells transfected with SLFN11-targeting small interfering RNAs (siRNAs) are reported. **n** Statistical analysis of tRNA levels, including six type II tRNAs and four type I tRNAs, in control and SLFN11-knockdown cells following IFN-α treatment using a two-sided paired Student's t-test. Each dot represents the mean of 3 biological replicates of give tRNA species. Source data are provided as a Source Data file.

Figure 3. **The tRNAome modulates the anti-HEV efficiency of interferon-alpha. a** Diagram illustrating tRNA maturation and charging, highlighting tRNA-

nucleotidyltransferase 1 (TRNT1) involvement. **b** Quantification of mature tRNA levels after siRNA-mediated knockdown of TRNT1 (n = 3). **c** Upon TRNT1 knockdown, the cells were treated with IFN-α followed by 48h of HEV infection (n = 3). Then, HEV RNA levels were quantified and compared. **d** Quantification of ISG mRNA levels after TRNT1 knockdown (n = 3). **e-f** Immunoblotting of ISG15 and IFIT3 after TRNT1 knockdown (e). After TRNT1 knockdown, immunoblotting of HEV ORF2 protein in IFN-α treated cells (f). Representative images from one of two independent experiments are shown. **g** Assessment of the impact of amino acid (AA) starvation on levels of non-charging tRNAs using a two-sided student's t-test for statistical analysis (n = 3); other tRNA species are provided in Supplementary Fig. 7a. **h** HEV infection performed on cells under either AA-limited (25%) or full medium conditions, followed by IFN-α treatment (n = 4). **i** In cells pretreated with IFN-α, AA-limited cells were treated for intervals of 4, 8, or 24 hours prior to HEV infection, while post-infection conditions involved IFN-α treatment for similar intervals; HEV RNA replication was assessed relative to normal culturing cells pretreated for 8 h of IFN-α, and a two-sided student's t-test for statistical analysis (n = 4). Center lines indicate the median; box limits indicate the 25th and 75th percentiles; whiskers extend to the minimum and maximum values, with all individual data points showed. **j** The AA-limited cells were transfected with or without TRNT1-targeting siRNA-2#, and infected by HEV. HEV replication in the cells with indicated conditions were statistically analyzed using a two-sided student's t-test (n = 3). **k** When recovering AA concentration from 25% to 100%, cells were infected and treated with IFN-α for indicated periods. HEV RNA loads were compared and analyzed with groups that were cultured in 25% medium using a two-sided student's t-test (n = 3 or 4). **l** Analysis of ISG15 and IFIT3 mRNA levels upon IFN-α treatment in cells cultured under different medium conditions (n = 3), as well as ATF4 and eIF2α. **m-n** Immunoblot analysis of IFIT3, ISG15, ATF4, and phosphorylated eIF2α performed under varying culture conditions upon IFN-α treatment, independently performed with 8, and 24 h of IFN-α treatment. Due to the low intensity of interested bands

at the 4h, these data are provided in the Source Data file. **o** Evaluation of the effects of individual AA supplementation on the anti-HEV properties of IFN-α (n = 3). **p** Immunoblot of HEV ORF2 proteins in cells cultured under varying medium conditions, independently performed with 4, 8, and 24 h of IFN-α treatment. Mean ± s.d. Source data are provided as a Source Data file.

Figure 4. **DHBV infection remodels the mature tRNAome without affecting the interferon-stimulated gene response. a-c** DHBV intracellular DNA levels (a) and pgRNA(pre-genomic RNA) transcription levels (b), and DHBV release in the supernatant (c) were assessed in human cells at 24 and 48 hpi using quantitative PCR (qPCR) and reverse-transcription qPCR (RT-qPCR) methods (n = 3). **d-f** In infected duck primary hepatocytes (DPH), DHBV intracellular DNA levels (d) and pgRNA transcription levels (e), and DHBV release in the supernatant (f) were similarly quantified at 24 and 48hpi (n = 3). **g** Staining of core protein in DHBV-infected Huh7 cells (two independent experiments). **h-i** The total mature tRNAome of humans (h) and ducks (i) was quantified at 24 and 48 hpi, normalized to levels in uninfected cells at the corresponding time points (set to 1.0) (n = 3)[17]. **j-k** Validation of notable ISGs' mRNA and protein levels upon DHBV infection in Huh7 cells. Cells treated with IFN-α or in combination with JAK (Janus kinase) inhibitor I (10 μM) served as control groups (n = 3). **l** Transcription levels of important ISGs in human cells infected with DHBV (n = 3) are shown. **m** Transcription levels of potential duck ISGs in duck cells infected with DHBV (n = 3). **n** Validation of notable ISG mRNA levels upon human HBV infection in Huh7-NTCP cells (n = 3). **o** Immunoblotting analysis of notable ISG protein levels and phosphorylation of STAT1 (signal transducer and activator of transcription 1) upon human HBV infection in Huh7-NTCP cells, independently at 24hpi and 48hpi. Mean ± s.d. Source data are provided as a Source Data file.

Figure 5. **Overexpression of tRNA-Arg-UCU 1-1 enhances DNA replication and**

DHBV core protein synthesis. a Sequence alignment showing human (h) and duck (d) tRNA-Arg-TCT genes. The secondary structure of human tRNA-Arg-UCU 1-1 is illustrated. **b** Quantification of five human tRNA-Arg-UCU levels in human cells after transduction with tRNA-expressing lentivirus, n = 4. **c** Measurement of DHBV DNA levels in infected human cells stably expressing the five human tRNA-Arg-UCU variants, assessed 48 hours post-infection (hpi) (n = 6). **d** Assessment of the impact of overexpressing the five human tRNA-Arg-UCU on DHBV core protein synthesis using Western blot analysis; a wild-type DHBV core protein plasmid with a Flag-tag was transfected into the selected human cell lines. **e** Quantification of tRNA-Arg-UCU levels following the transfection of three duck tRNA-Arg-UCU variants in DPHs (n = 6). **f** Evaluation of the influence of the three duck tRNA-Arg-UCU variants on DHBV DNA replication in infected DPHs (n = 6). **g** Effect of the three duck tRNA-Arg-UCU variants on DHBV core protein synthesis in DPHs; DPHs were first transfected with tRNA overexpression plasmids, then a wild-type DHBV Flag-tagged core protein plasmid, followed by detection of core protein expression through blotting analysis. Mean ± s.d. Source data are provided as a Source Data file.

Figure 6. **Functional inhibition of tRNA-Arg-UCU reduces replicative capacity of DHBV. a** Schematic illustration depicting the mature tRNA statuses, in which only charged tRNA (aminoacylated) is functionally engaged in translational decoding, while uncharged tRNA remains inactive. **b** The effects of arginine deprivation and subsequent replenishment on levels of uncharged tRNA-Arg-UCU in human cells are shown (n = 4). **c** Quantification of DHBV DNA replication in arginine-depleted cultured human cells, both before and after adding back the depleted arginine in the culture medium (n = 4). **d** Impact of arginine deprivation and replenishment on uncharged tRNA-Arg-UCU levels in duck hepatocytes (n = 3). **e** Effects of arginine levels on DHBV DNA replication in the same duck hepatocyte model (n = 3). **f** Human cell clones were established post-transduction with lentiviruses carrying tRNA-Arg-UCU 1-1, tRNAm-Ala-UCU, and tRNA-Ser-UGA;

levels of tRNA species were quantified and compared to control (vec) groups (n = 5, 6). **g** Analysis of DHBV DNA replication in infected human cell clones expressing tRNA-Arg-UCU 1-1, tRNAm-Ala-UCU, and tRNA-Ser-UGA (n = 6). **h** Assessment of DHBV core protein synthesis in the same cell clones was performed via western blot analysis. **i** Indirect immunofluorescence assay (IFA) results for DHBV core protein synthesis in the infected clones. **j** Duck hepatocytes were transfected with plasmids encoding tRNA-Arg-UCU 1-1, tRNAm-Ala-UCU, and tRNA-Ser-UGA (2 μg/well) using the PEI transfection method, with subsequent quantification of transfected tRNA levels compared to mock and untransfected groups (n = 5, 6). **k** Following transfection, replication levels of DHBV in infected duck hepatocytes expressing tRNA species were evaluated (n = 6). **l** DHBV core protein synthesis was measured in these hepatocytes using western blotting. **m** IFA was employed to assess DHBV core protein synthesis in the infected duck hepatocytes. Mean ± s.d. Source data are provided as a Source Data file.

Figure 7. **The tRNA-Arg-UCU translational advantage requires AGA codons in core protein genes and influences pgRNA transcription. a** Construction of a wild-type (WT) vector and a vector with all AGA codons replaced by AGG, expressing duck hepatitis B virus (DHBV) core protein. **b** In human cells, the AGA>AGG mutation completely inhibited core protein synthesis in both tRNA-Arg-UCU 1-1 overexpressing and control vector groups. Overexpression of tRNA-Arg-UCU 1-1 significantly increased DHBV core protein synthesis compared to the vector group for the WT core protein gene. **c** In duck hepatocytes, similar results were observed, confirming the findings in human cells. **d** Schematic representation indicating that tRNA-Arg-UCU-mediated core protein synthesis affects HBV DNA replication and may indirectly regulate pgRNA transcription. The decoding of pgRNA transcripts leads to core protein synthesis, which is regulated by tRNA-Arg-UCU 1-1. The assembled core proteins create nucleocapsids for HBV pgRNA packaging; the synthesized double-stranded viral DNA serves as a template for pgRNA

transcription, suggesting a potential role for tRNA-Arg-UCU in regulating this process. **e** Diagram illustrating functional domains of the DHBV core protein involved in pgRNA packaging: the assembly domain promotes nucleocapsid assembly, while the C-terminal arginine-rich domain is crucial for pgRNA interaction. **f-g** The effect of tRNA-Arg-UCU on pgRNA transcription measured by reverse transcription quantitative polymerase chain reaction (RT-qPCR) in infected human cells (f) and duck hepatocytes (g) (n = 6). **h-i** Comparison of the impacts of tRNA-Arg-UCU and non-cognate tRNA-Ser-UGA on pgRNA transcription in infected human cells (h) and duck hepatocytes (i) (n = 5, 6). **j-k** After 48 hours of DHBV infection, pgRNA transcription levels were quantified in arginine-depleted Huh7 cells (j) and duck hepatocytes (k), with subsequent restoration of arginine assessed (n = 4). Mean ± s.d. Source data are provided as a Source Data file.

Figure 8. **Validation of the role of tRNA-Arg-UCU in human HBV-NTCP cells and an Alb-Cre transgenic HBV mouse model. a** Quantification of intracellular HBV DNA and pgRNA levels in HBV-infected NTCP stably expressed human hepatocytes transfected with tRNA-Arg-UCU 1-1 or vector plasmids (n = 5, 6). **b** Immunofluorescent staining showing HBV core protein expression in hepatocytes transfected with either tRNA-Arg-UCU 1-1 or vector plasmids under the same conditions as in panel a. **c** Assessment of the impact of entecavir (ETV) on HBV DNA replication and pgRNA transcription in cells transfected with tRNA-Arg-UCU 1-1 (n = 5, 6). **d** Experimental design: Alb-Cre transgenic mice were used to generate an HBV infection model. Mice with HBV blood titers approximately 1.0×10^4 copies/mL were intravenously administered 50 μL of lentivirus containing 1.0×10^9 copies of either tRNA-Arg-UCU 1-1 or a scrambled vector sequence. After 1 week, liver tissues were collected for histological and virological examinations. **e** Hematoxylin and eosin (HE) staining of HBV-infected liver tissues transducing tRNA-Arg-UCU 1-1 or vector, displaying three representative images. **f** Blood test results for alanine aminotransferase (ALT) and aspartate aminotransferase (AST) at the time of sampling. A

two-sided student's t-test was used for statistical analysis (n = 6). **g** Immunochemical staining revealing HBV core proteins in liver tissues, with brown indicating positive staining. **h** Quantification of HBV DNA levels in mouse livers transducing tRNA-Arg-UCU 1-1 or vector after one week using a one-side student's t-test (n = 6, 7); prior to lentiviral transduction, HBV DNA levels in blood were comparable between groups. Mean ± s.d. Source data are provided as a Source Data file.

Figure 9. **The dual role of the mature tRNAome in the interferon-mediated antiviral response and HBV infection.** Mature tRNAome facilitates the translational decoding of virtually all mRNAs, regardless of whether they are derived from the host or from viruses. Left panel illustrates the remodeling of the mature tRNAome by IFN-α, which influences the translational decoding of interferon-stimulated genes (ISGs), thereby modulating the overall host antiviral response. Right panel depicts the impact of HBV infection, which does not promote ISG transcription but alters the host mature tRNAome. The identified upregulation of the host tRNA-Arg-UCU is shown to significantly enhance various stages of HBV infection, from core protein synthesis to DNA replication and the transcription of viral pgRNA.

Editorial Summary

The role of the tRNAome in virus-host interaction is poorly understood. Here, the authors report a dual role of the host tRNAome showing that it is remodeled by IFN-α to regulate antiviral defenses, yet can be exploited by hepatitis viruses to benefit infection, particularly when host antiviral responses are not induced.

Peer review information: *Nature Communications* thanks Sumana Sanyal and the other anonymous reviewer(s) for their contribution to the peer review of this work. A peer review file is available.

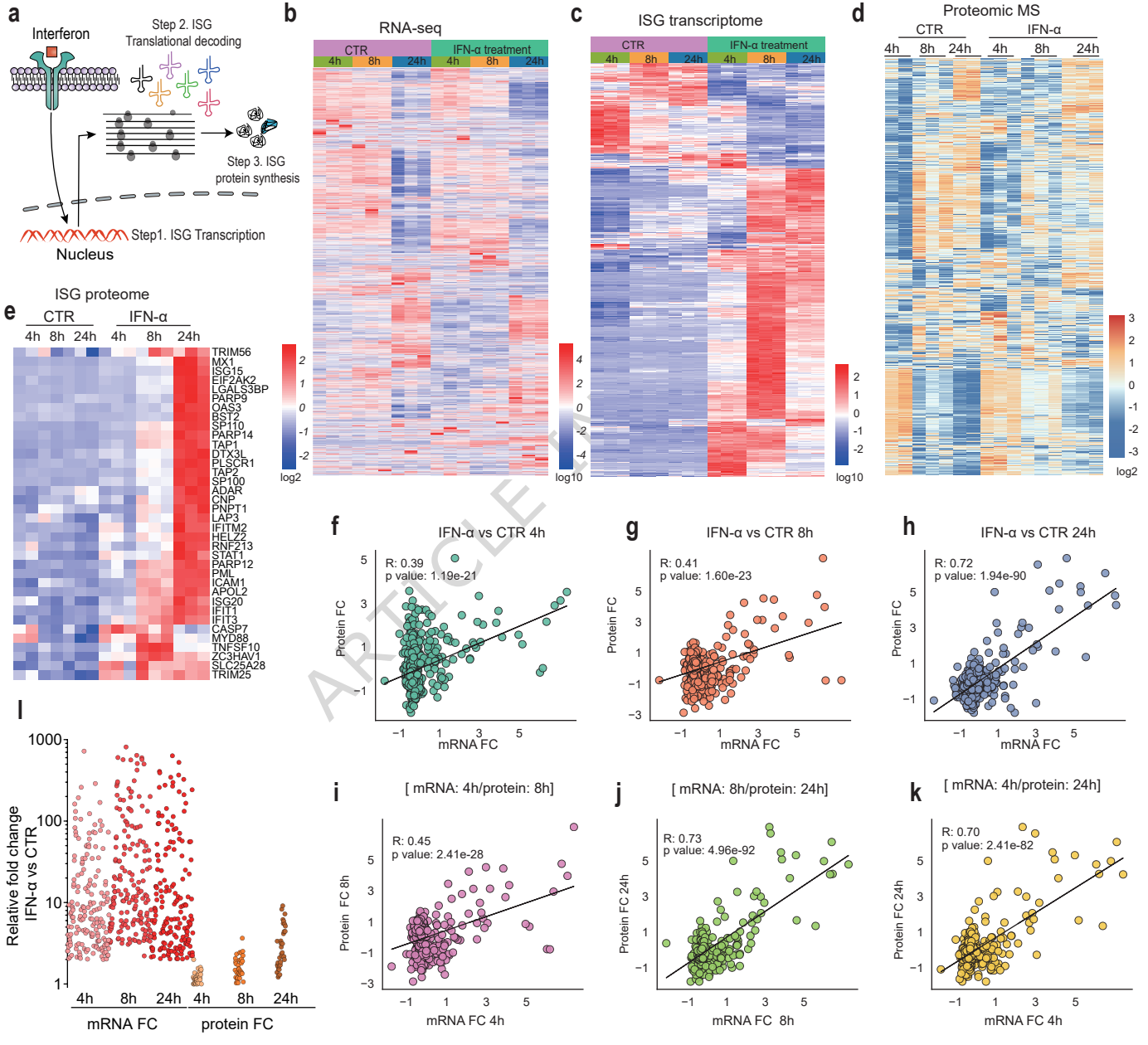
a
Interferon
Step 2. ISG
Translational decoding
Step 3. ISG
protein synthesis
Step1. ISG Transcription
Nucleus
b
RNA-seq
CTR
IFN-α treatment
4h 8h 24h 4h 8h 24h
log2
c
ISG transcriptome
CTR
IFN-α treatment
4h 8h 24h 4h 8h 24h
log10
d
Proteomic MS
CTR
IFN-α
4h 8h 24h 4h 8h 24h
log2
e
ISG proteome
CTR
IFN-α
4h 8h 24h 4h 8h 24h
TRIM56
MX1
ISG15
EIF2AK2
LGALS3BP
PARP9
OAS3
BST2
SP110
PARP14
TAP1
DTX3L
PLSCR1
TAP2
SP100
ADAR
CNP
PNPT1
LAP3
IFITM2
HELZ2
RNF213
STAT1
PARP12
PML
ICAM1
APOL2
ISG20
IFIT1
IFIT3
CASP7
MYD88
TNFSF10
ZC3HAV1
SLC25A28
TRIM25
f
IFN-α vs CTR 4h
R: 0.39
p value: 1.19e-21
Protein FC
mRNA FC
g
IFN-α vs CTR 8h
R: 0.41
p value: 1.60e-23
Protein FC
mRNA FC
h
IFN-α vs CTR 24h
R: 0.72
p value: 1.94e-90
Protein FC
mRNA FC
i
[mRNA: 4h/protein: 8h]
R: 0.45
p value: 2.41e-28
Protein FC 8h
mRNA FC 4h
j
[mRNA: 8h/protein: 24h]
R: 0.73
p value: 4.96e-92
Protein FC 24h
mRNA FC 8h
k
[mRNA: 4h/protein: 24h]
R: 0.70
p value: 2.41e-82
Protein FC 24h
mRNA FC 4h
l
Relative fold change
IFN-α vs CTR
4h 8h 24h 4h 8h 24h
mRNA FC
protein FC

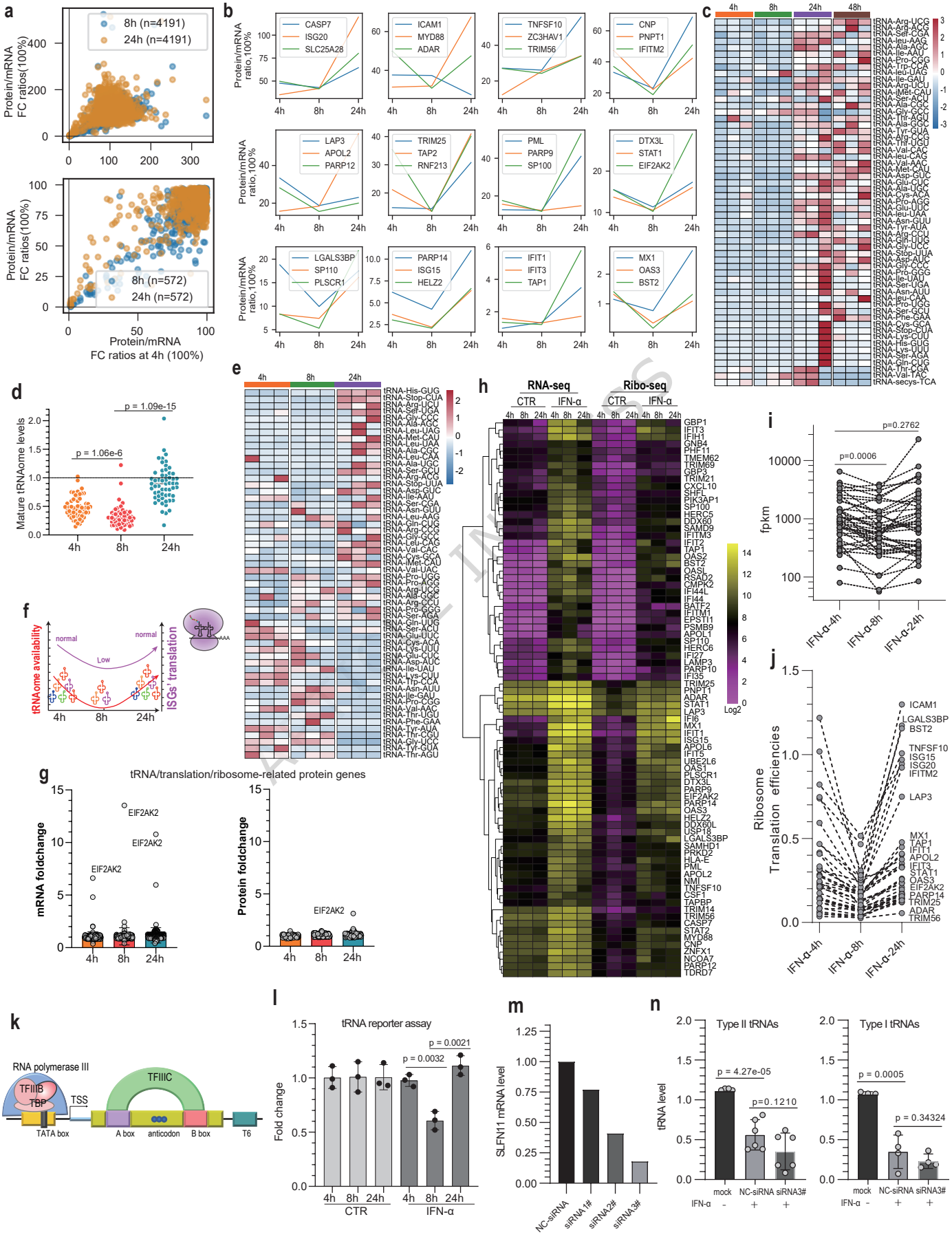
a
8h (n=4191)
24h (n=4191)
Protein/mRNA FC ratios(100%)
8h (n=572)
24h (n=572)
Protein/mRNA FC ratios at 4h (100%)
b
Protein/mRNA ratio,100%
CASP7
ISG20
SLC25A28
ICAM1
MYD88
ADAR
TNFSF10
ZC3HAV1
TRIM56
CNP
PNPT1
IFITM2
LAP3
APOL2
PARP12
TRIM25
TAP2
RNF213
PML
PARP9
SP100
DTX3L
STAT1
EIF2AK2
LGALS3BP
SP110
PLSCR1
PARP14
ISG15
HELZ2
IFIT1
IFIT3
TAP1
MX1
OAS3
BST2
c
4h
8h
24h
48h
d
Mature tRNAome levels
p = 1.09e-15
p = 1.06e-6
e
f
tRNAome availability
normal
Low
normal
ISGs' translation
g
tRNA/translation/ribosome-related protein genes
mRNA foldchange
Protein foldchange
EIF2AK2
h
RNA-seq
Ribo-seq
CTR
IFN-α
Log2
i
fpkm
p=0.2762
p=0.0006
IFN-α-4h
IFN-α-8h
IFN-α-24h
j
Ribosome Translation efficiencies
k
RNA polymerase III
TFIIIB
TBP
TSS
TFIIIC
TATA box
A box
anticodon
B box
T6
l
tRNA reporter assay
Fold change
p = 0.0021
p = 0.0032
CTR
IFN-α
m
SLFN11 mRNA level
NC-siRNA
siRNA 1#
siRNA2#
siRNA3#
n
Type II tRNAs
Type I tRNAs
tRNA level
p = 4.27e-05
p=0.1210
p = 0.0005
p = 0.34324
mock
NC-siRNA
siRNA3#
IFN-α

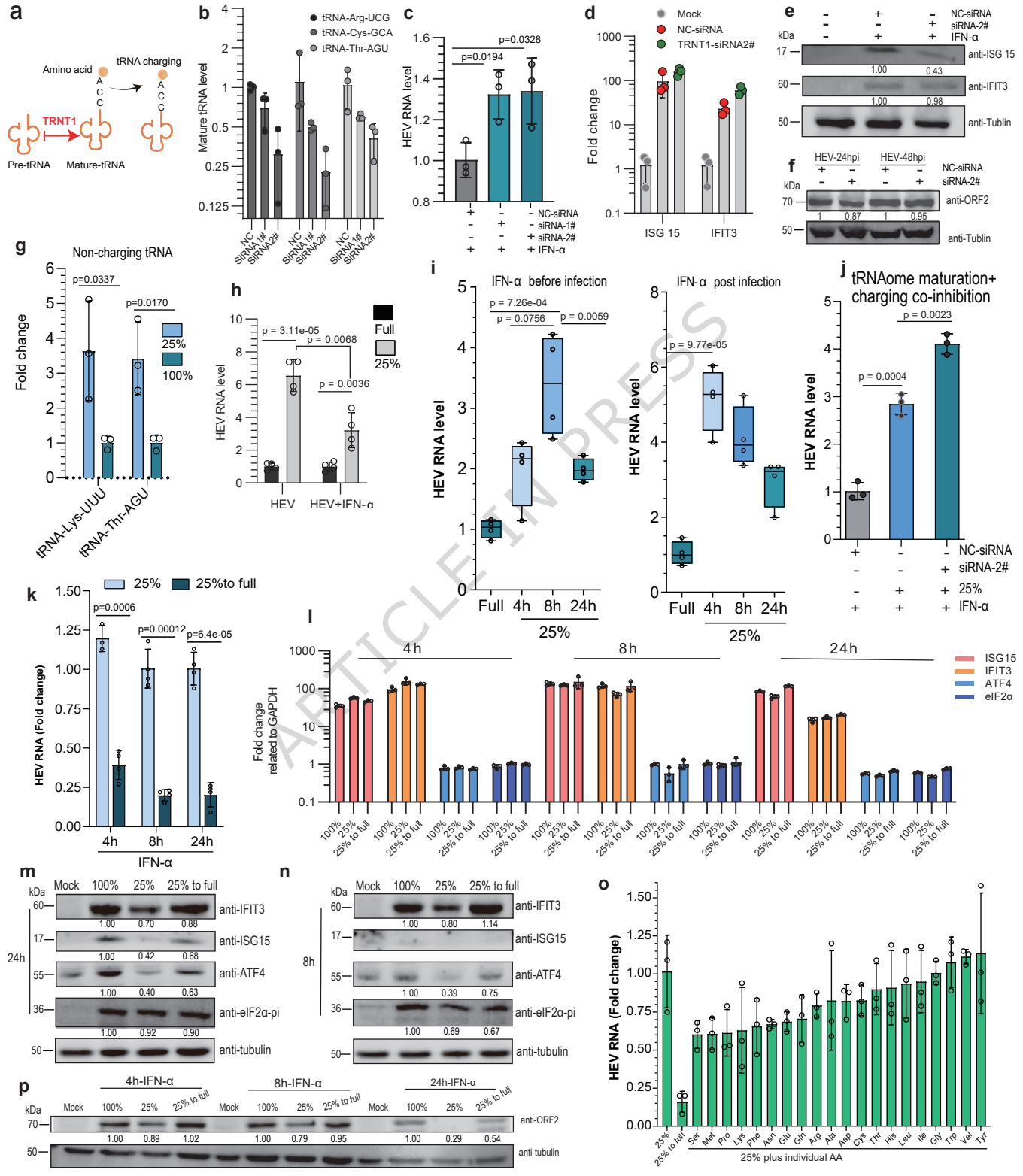

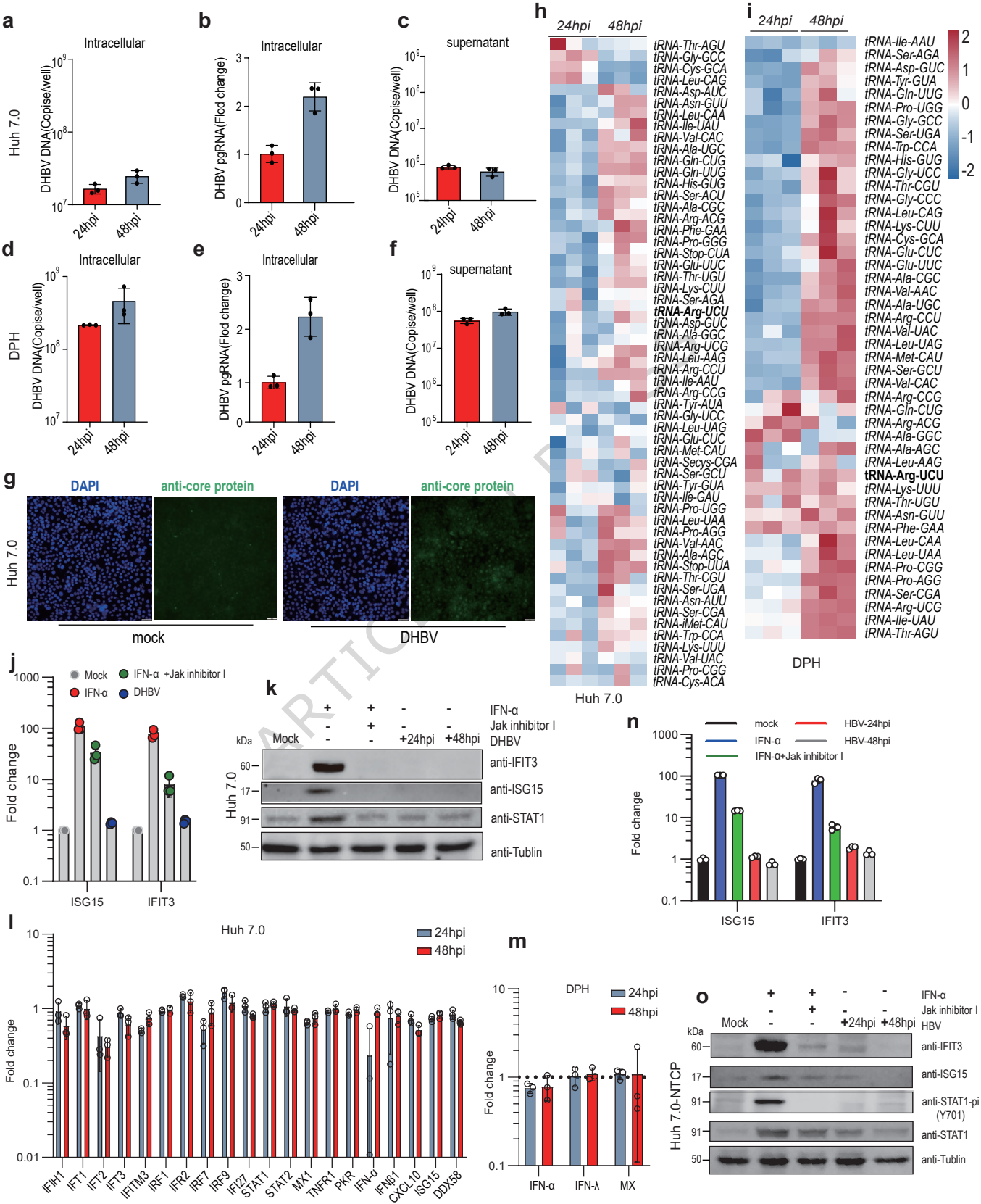
a
Intracellular
Huh 7.0
DHBV DNA(Copise/well)
24hpi
48hpi
b
Intracellular
DHBV pgRNA(Flod change)
c
supernatant
DHBV DNA(Copise/well)
d
Intracellular
DPH
e
Intracellular
f
supernatant
g
DAPI
anti-core protein
mock
DHBV
h
24hpi
48hpi
tRNA-Thr-AGU
tRNA-Gly-GCC
tRNA-Cys-GCA
tRNA-Leu-CAG
tRNA-Asp-AUC
tRNA-Asn-GUU
tRNA-Leu-CAA
tRNA-Ile-UAU
tRNA-Val-CAC
tRNA-Ala-UGC
tRNA-Gln-CUG
tRNA-Gln-UUG
tRNA-His-GUG
tRNA-Ser-ACU
tRNA-Ala-CGC
tRNA-Arg-ACG
tRNA-Phe-GAA
tRNA-Pro-GGG
tRNA-Stop-CUA
tRNA-Glu-UUC
tRNA-Thr-UGU
tRNA-Lys-CUU
tRNA-Ser-AGA
tRNA-Arg-UCU
tRNA-Asp-GUC
tRNA-Ala-GGC
tRNA-Arg-UCG
tRNA-Leu-AAG
tRNA-Arg-CCU
tRNA-Ile-AAU
tRNA-Arg-CCG
tRNA-Tyr-AUA
tRNA-Gly-UCC
tRNA-Leu-UAG
tRNA-Glu-CUC
tRNA-Met-CAU
tRNA-Secys-CGA
tRNA-Ser-GCU
tRNA-Tyr-GUA
tRNA-Ile-GAU
tRNA-Pro-UGG
tRNA-Leu-UAA
tRNA-Pro-AGG
tRNA-Val-AAC
tRNA-Ala-AGC
tRNA-Stop-UUA
tRNA-Thr-CGU
tRNA-Ser-UGA
tRNA-Asn-AUU
tRNA-Ser-CGA
tRNA-iMet-CAU
tRNA-Trp-CCA
tRNA-Lys-UUU
tRNA-Val-UAC
tRNA-Pro-CGG
tRNA-Cys-ACA
Huh 7.0
i
24hpi
48hpi
tRNA-Ile-AAU
tRNA-Ser-AGA
tRNA-Asp-GUC
tRNA-Tyr-GUA
tRNA-Gln-UUG
tRNA-Pro-UGG
tRNA-Gly-GCC
tRNA-Ser-UGA
tRNA-Trp-CCA
tRNA-His-GUG
tRNA-Gly-UCC
tRNA-Thr-CGU
tRNA-Gly-CCC
tRNA-Leu-CAG
tRNA-Lys-CUU
tRNA-Cys-GCA
tRNA-Glu-CUC
tRNA-Glu-UUC
tRNA-Ala-CGC
tRNA-Val-AAC
tRNA-Ala-UGC
tRNA-Arg-CCU
tRNA-Val-UAC
tRNA-Leu-UAG
tRNA-Met-CAU
tRNA-Ser-GCU
tRNA-Val-CAC
tRNA-Arg-CCG
tRNA-Gln-CUG
tRNA-Arg-ACG
tRNA-Ala-GGC
tRNA-Ala-AGC
tRNA-Leu-AAG
tRNA-Arg-UCU
tRNA-Lys-UUU
tRNA-Thr-UGU
tRNA-Asn-GUU
tRNA-Phe-GAA
tRNA-Leu-CAA
tRNA-Leu-UAA
tRNA-Pro-CGG
tRNA-Pro-AGG
tRNA-Ser-CGA
tRNA-Arg-UCG
tRNA-Ile-UAU
tRNA-Thr-AGU
DPH
j
Mock
IFN-α
IFN-α +Jak inhibitor I
DHBV
Fold change
ISG15
IFIT3
k
IFN-α
Jak inhibitor I
DHBV
Mock
+24hpi
+48hpi
kDa
anti-IFIT3
anti-ISG15
anti-STAT1
anti-Tublin
Huh 7.0
n
mock
IFN-α
IFN-α+Jak inhibitor I
HBV-24hpi
HBV-48hpi
Fold change
ISG15
IFIT3
l
Huh 7.0
24hpi
48hpi
Fold change
IFIH1
IFT1
IFT2
IFT3
IFITM3
IRF1
IFR2
IRF7
IRF9
IFI27
STAT1
STAT2
MX1
TNFR1
PKR
IFN-α
IFNß1
CXCL10
ISG15
DDX58
m
DPH
24hpi
48hpi
Fold change
IFN-α
IFN-λ
MX
o
IFN-α
Jak inhibitor I
HBV
Mock
+24hpi
+48hpi
kDa
anti-IFIT3
anti-ISG15
anti-STAT1-pi (Y701)
anti-STAT1
anti-Tublin
Huh 7.0-NTCP

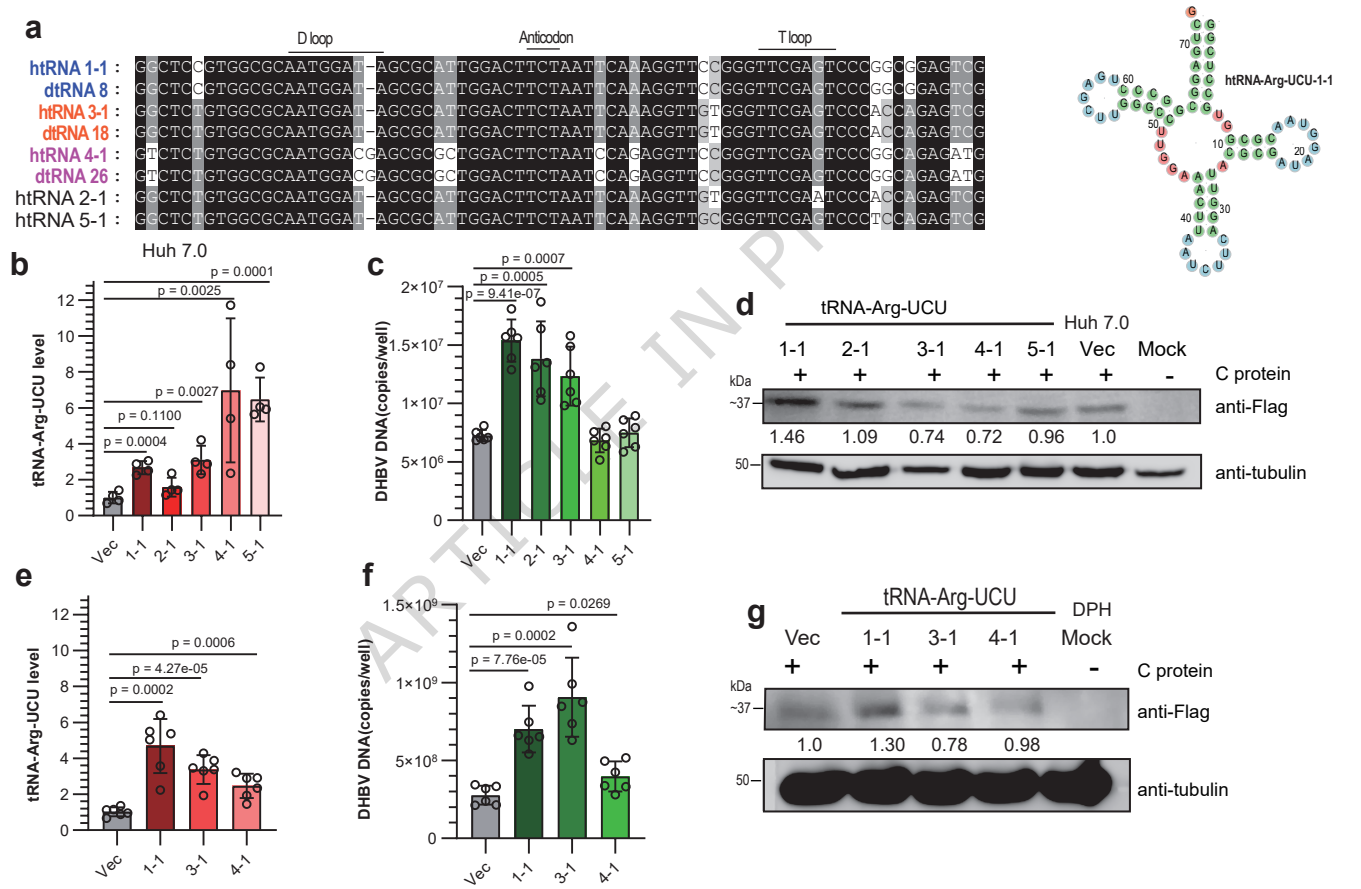

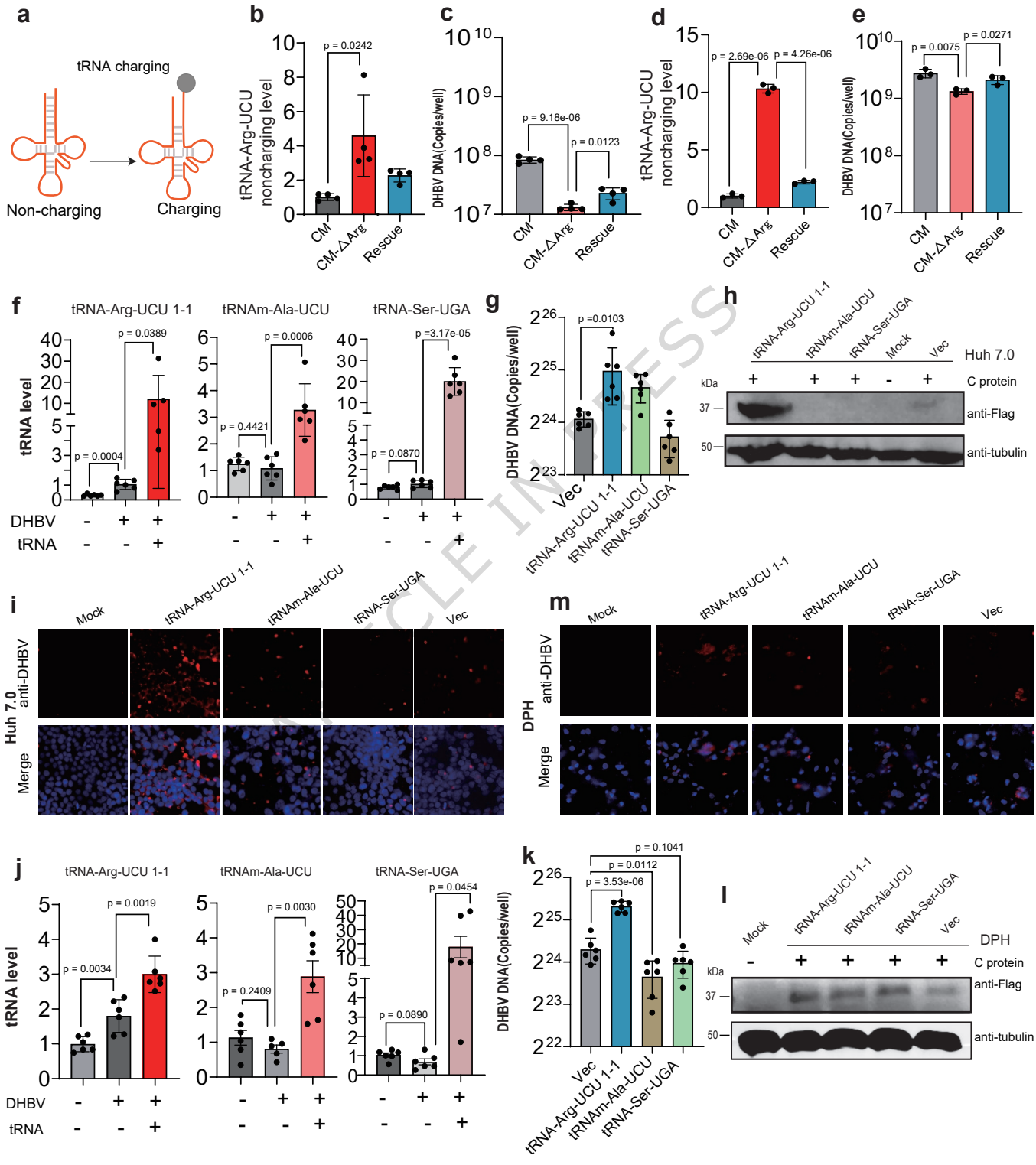
a
tRNA charging
Non-charging
Charging
b
tRNA-Arg-UCU noncharging level
p = 0.0242
CM
CM-ΔArg
Rescue
c
DHBV DNA(Copies/well)
p = 9.18e-06
p = 0.0123
d
tRNA-Arg-UCU noncharging level
p = 2.69e-06
p = 4.26e-06
e
DHBV DNA(Copies/well)
p = 0.0075
p = 0.0271
f
tRNA-Arg-UCU 1-1
tRNAm-Ala-UCU
tRNA-Ser-UGA
tRNA level
p = 0.0004
p = 0.0389
p = 0.4421
p = 0.0006
p = 0.0870
p =3.17e-05
DHBV
tRNA
g
DHBV DNA(Copies/well)
p =0.0103
Vec
tRNA-Arg-UCU 1-1
tRNAm-Ala-UCU
tRNA-Ser-UGA
h
Mock
Vec
Huh 7.0
C protein
kDa
37
50
anti-Flag
anti-tubulin
i
Mock
Vec
Huh 7.0
anti-DHBV
Merge
m
DPH
j
p = 0.0034
p = 0.0019
p = 0.2409
p = 0.0030
p = 0.0890
p = 0.0454
k
p = 0.1041
p = 0.0112
p = 3.53e-06
l

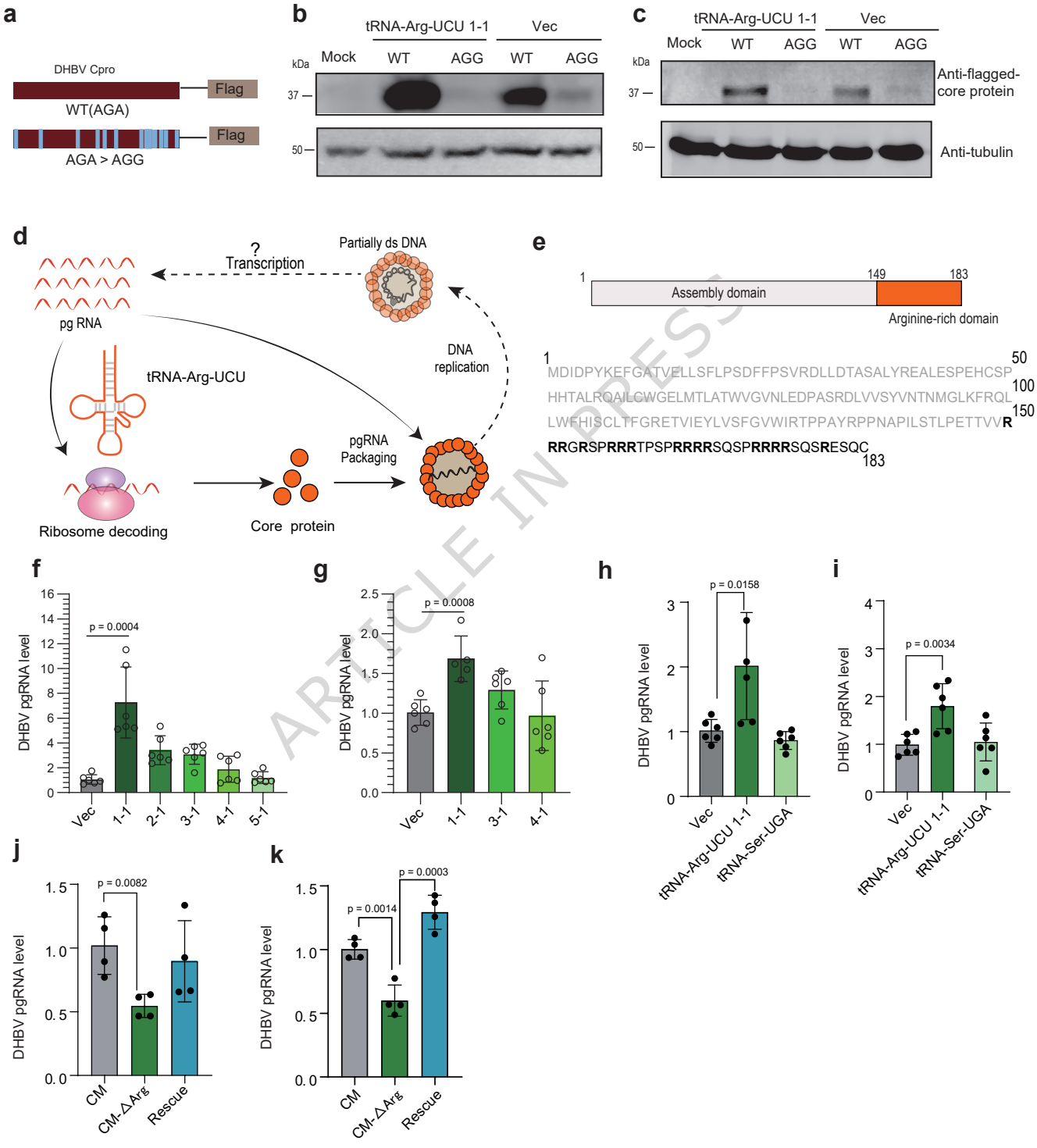
a
DHBV Cpro
Flag
WT(AGA)
Flag
AGA > AGG
b
tRNA-Arg-UCU 1-1
Vec
kDa
Mock
WT
AGG
WT
AGG
37
50
c
tRNA-Arg-UCU 1-1
Vec
Mock
WT
AGG
WT
AGG
kDa
37
50
Anti-flagged-core protein
Anti-tubulin
d
?
Transcription
Partially ds DNA
pg RNA
DNA replication
tRNA-Arg-UCU
pgRNA Packaging
Ribosome decoding
Core protein
e
1
149
183
Assembly domain
Arginine-rich domain
1
50
MDIDPYKEFGATVELLSFLPSDFFPSVRDLLDTASALYREALESPEHCSP
100
HHTALRQAILCWGELMTLATWVGVNLEDPASRDLVVSYVNTNMGLKFRQL
150
LWFHISCLTFGRETVIEYLVSFGVWIRTPPAYRPPNAPILSTLPETTVV
R
RRGRSPRRRTPSPRRRRSQSPRRRRSQSRESQC
183
f
DHBV pgRNA level
p = 0.0004
Vec
1-1
2-1
3-1
4-1
5-1
g
DHBV pgRNA level
p = 0.0008
Vec
1-1
3-1
4-1
h
DHBV pgRNA level
p = 0.0158
Vec
tRNA-Arg-UCU 1-1
tRNA-Ser-UGA
i
DHBV pgRNA level
p = 0.0034
Vec
tRNA-Arg-UCU 1-1
tRNA-Ser-UGA
j
DHBV pgRNA level
p = 0.0082
CM
CM-ΔArg
Rescue
k
DHBV pgRNA level
p = 0.0014
p = 0.0003
CM
CM-ΔArg
Rescue

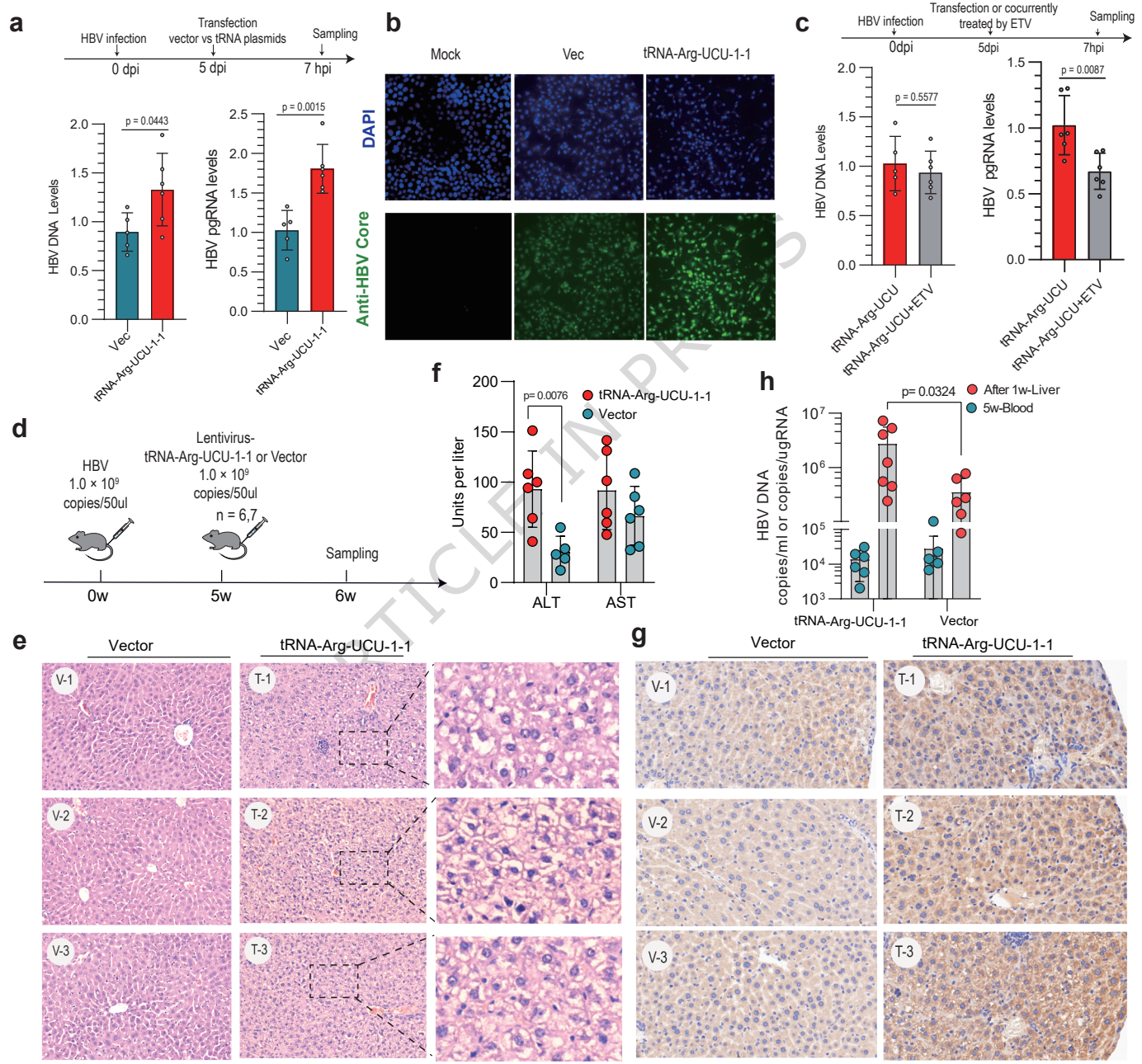
a
HBV infection
Transfection
vector vs tRNA plasmids
Sampling
0 dpi
5 dpi
7 hpi
HBV DNA Levels
p = 0.0443
Vec
tRNA-Arg-UCU-1-1
HBV pgRNA levels
p = 0.0015
b
Mock
Vec
tRNA-Arg-UCU-1-1
DAPI
Anti-HBV Core
c
HBV infection
Transfection or cocurrently treated by ETV
Sampling
0dpi
5dpi
7hpi
HBV DNA Levels
p = 0.5577
HBV pgRNA levels
p = 0.0087
tRNA-Arg-UCU
tRNA-Arg-UCU+ETV
d
HBV
1.0 × 10⁹ copies/50ul
Lentivirus-
tRNA-Arg-UCU-1-1 or Vector
1.0 × 10⁹ copies/50ul
n = 6,7
Sampling
0w
5w
6w
f
p= 0.0076
tRNA-Arg-UCU-1-1
Vector
Units per liter
ALT
AST
h
p= 0.0324
After 1w-Liver
5w-Blood
HBV DNA copies/ml or copies/ugRNA
tRNA-Arg-UCU-1-1
Vector
e
Vector
tRNA-Arg-UCU-1-1
V-1
T-1
V-2
T-2
V-3
T-3
g
Vector
tRNA-Arg-UCU-1-1
V-1
T-1
V-2
T-2
V-3
T-3